FIBER-INTEGRATED TERAHERTZ SPECTROMETER DRIVEN BY ULTRAFAST YTTERBIUM DOPED FIBER LASER

A THESIS SUBMITTED TO
THE GRADUATE SCHOOL OF NATURAL AND APPLIED SCIENCES
OF
MIDDLE EAST TECHNICAL UNIVERSITY

HAKAN KESKIN

IN PARTIAL FULFILLMENT OF THE REQUIREMENTS
FOR
THE DEGREE OF MASTER OF SCIENCE
IN
PHYSICS

SEPTEMBER 2013

Approval of the thesis:

FIBER-INTEGRATED TERAHERTZ SPECTROMETER DRIVEN BY ULTRAFAST YTTERBIUM DOPED FIBER LASER

submitted by **HAKAN KESKIN** in partial fulfillment of the requirements for the degree of **Master of Science in Physics Department, Middle East Technical University** by,

Prof. Dr. Canan Özgen _____
Dean, Graduate School of **Natural and Applied Sciences**

Prof. Dr. Mehmet T. Zeyrek _____
Head of Department, **Physics**

Assoc. Prof. Dr. Hakan Altan _____
Supervisor, **Physics Department, METU**

Dr. Halil Berberoğlu _____
Co-supervisor, **Physics Department, METU**

Examining Committee Members:

Assoc. Prof. Dr. Hakan Altan
Physics Department,METU _____

Assist. Prof. Dr. F. Ömer İlday
Physics Department, Bilkent University _____

Dr. Halil Berberoğlu
Physics Department, METU _____

Assist. Prof. Dr. Alpan Bek
Physics Department,METU _____

Assist. Prof. Dr. Asaf Behzat Şahin
Electrical and Communication Engineering Department, Yıldırım Beyazıt University
_____

Date: _____

I hereby declare that all information in this document has been obtained and presented in accordance with academic rules and ethical conduct. I also declare that, as required by these rules and conduct, I have fully cited and referenced all material and results that are not original to this work.

Name, Last Name: HAKAN KESKIN

Signature :

ABSTRACT

FIBER-INTEGRATED TERAHERTZ SPECTROMETER DRIVEN BY ULTRAFAST YTTERBIUM DOPED FIBER LASER

Keskin, Hakan
M.S., Department of Physics
Supervisor : Assoc. Prof. Dr. Hakan Altan
Co-Supervisor : Dr. Halil Berberoğlu

September 2013, 63 pages

In this thesis, development of a Terahertz time domain spectrometer (THz-TDS) driven by an ultrafast Ytterbium (Yb) doped fiber laser, whose repetition rate can be tuned, was investigated to show that it can be used in Optical Sampling by Cavity Tuning (OSCAT) technique which enables the fast acquisition of THz pulse profiles. Central wavelength of the Yb-doped laser developed for this study is 1031 nm. The output average power was measured to be 90 mW which corresponds to about two nanojoule per pulse at 51 MHz repetition rate, and the pulse duration was measured with an autocorrelator to be ∼80 fs. Average output power and pulse duration stability of Yb-doped fiber laser oscillator was examined at different repetition rates in order to test convenience of system for THz measurements. By tuning the repetition rate at 51 MHz by ±25 kHz, we can scan a 100 ps time-window for the THz pulse measurement. This corresponded to a 6 mm cavity length tuning which altered the repetition rate of oscillator from by 53 kHz. Afterwards, THz-TDS system was built to understand the dependence of THz pulse profile on the repetition rate of the Yb-doped fiber laser. In this system InGaAs based photoconductive antenna (PCA) was used for

THz generation and 2 mm thick <110> orientation ZnTe crystal was used in the detection part. Due to the limitation of the balanced photodetector with respect to the central wavelength of the laser, only a bandwidth up to 0.5 THz with a signal to noise ratio(S/N) of ∼60 was observed. THz signals measured at different cavity lengths overlap in both time domain and magnitudes which mean that THz measurements were not affected by tuning the repetition rate of Yb-doped fiber laser. In order to achieve this result, source parameters such as pulse duration and power of Yb-doped fiber laser should be constant between measurements while scanning cavity length. By comparing THz signals at different repetition rates, it was shown that repetition rate tuning of Yb-doped oscillator can be used in OSCAT technique. In other words, we have shown that a Yb-doped fiber laser can be used to rapidly scan the THz pulse profile for future measurements.

Keywords: Terahertz, TDS , Fiber, Laser, Repetition Rate

ÖZ

İTERBİYUM KATKILI FİBER LAZERLE TÜMLEŞİK TERAHERTZ SPEKTROMETRE

Keskin, Hakan
Yüksek Lisans, Fizik Bölümü
Tez Yöneticisi : Doç. Dr. Hakan Altan
Ortak Tez Yöneticisi : Dr. Halil Berberoğlu

Eylül 2013 , 63 sayfa

Bu tezde, tekrarlama frekansı değiştirilebilen, çok kısa atımlı iterbiyum (Yb) katkılı fiber lazerin, kavite uzunluğu ayarlanarak terahertz atım profili ölçüm tekniğinde (OSCAT) kullanılabilir olduğunu göstermek için, bu lazer tarafından sürülen Zamana Bağlı Terahertz Spektrometre (THz-TDS) sistemi incelenecektir. Bu çalışma için geliştirilen Yb-katkılı lazerin merkez dalga boyu 1031 nm'dir. Ölçülen çıkış gücü, 51 MHz tekrarlama frekansında yaklaşık iki nanojule denk gelen 90 mW'tır ve otokorelatör ile ölçülen atım uzunluğu ∼80 fs'dir. Sistemin, THz ölçümleri için uygunluğunu test etmek amacıyla çıkış gücü ve atım uzunluğu kararlılığı farklı tekrarlama frekanslarında incelenmiştir. 51 MHz olan tekrarlama frekansı, THz atım ölçümlerinde 100 ps tarama yapabilmek için ±25 kHz ayarlanmalıdır. 6 mm kavite uzunluğuna denk gelen bu ayarlama, lazerin tekrarlama frekansını 53 kHz kadar değiştirmektedir. Daha sonra, Yb-katkılı fiber lazerin tekrarlama frekansının THz atım profiline etkisini anlamak için THz-TDS sistemi kurulmuştur. Bu sistemde, THz üretmek için InGaAs tabanlı fotoiletken anten, tespit bölümünde ise 2 mm kalınlığında <110> oryantasyonunda ZnTe kristali

kullanılmıştır. Dengeli fotodetektörün lazer merkez dalga boyundaki kısıtlamalarından dolayı sadece ∼60 sinyal/gürültü oranıyla 0.5 THz kadar bant genişliği gözlemlenmiştir. Farklı kavite uzunluklarında ölçülen THz sinyalleri, zamanda ve büyüklükte kesişmektedirler. Yani THz ölçümleri, Yb-katkılı fiber lazerin tekrarlama frekansının değiştirilmesinden etkilenmemiştir. Böyle bir sonuca ulaşabilmek için, Yb katkılı fiber lazerin atım uzunluğu ve güç gibi parametrelerinin sabit kalması gerekmektedir. Farklı tekrarlama frekanslarındaki THz sinyallerini karşılaştırarak, Yb katkılı lazerin tekrarlama frekansını değiştirme yönteminin, OSCAT tekniğinde kullanılabileceği gösterilmiştir. Diğer bir deyişle, Yb-katkılı fiber lazerin gelecekteki hızlı THz atım profili ölçümlerinde kullanılabileceğini göstermiş olduk.

Anahtar Kelimeler: Terahertz, Zamana Bağlı Spektrometre, Fiber, Lazer, Tekrarlama Frekansı

To my dear Family

ACKNOWLEDGMENTS

I am most thankful to my supervisor Assoc. Prof. Dr. Hakan Altan and my co-supervisor Dr. Halil Berberoğlu for sharing their invaluable ideas and experiences on the subject of my thesis.

I am very grateful to FiberLAST and UFOLAB throughout the production of laser.

I am indebted to Seydi Yavaş and Zeynep Özer, for their close collaboration when developing the laser and terahertz systems.

I would like to forward my appreciation to all my friends and colleagues especially Koray Eken, Assoc. Prof. Dr. F. Ömer İlday and Kamil Çınar, Yakup Midilli, Mahmut Emre Yağcı, Yiğit Ozan Aydın, Mesut Tasalı who contributed to my thesis with their continuous encouragement.

This work was supported by The Scientific And Technological Research Council Of Turkey (TUBITAK) under grant number 111T748.

TABLE OF CONTENTS

ABSTRACT iv

ÖZ vi

ACKNOWLEDGMENTS ix

TABLE OF CONTENTS x

LIST OF TABLES xii

LIST OF FIGURES xiii

LIST OF ABBREVIATIONS xv

CHAPTERS

1 INTRODUCTION 1

1.1 TERAHERTZ TIME DOMAIN SPECTROSCOPY 4

1.2 ULTRAFAST FIBER LASERS 6

2 BACKGROUND OF FIBER LASER 9

2.1 OPTICAL FIBERS 9

2.2 DISPERSION 10

2.3 NONLINEAR OPTICS IN FIBER 12

2.4 PULSE PROPAGATION IN FIBER 14

2.5 MODE LOCKING THEORY 14

2.6 NUMERICAL SIMULATIONS OF OSCILLATOR 16

2.6.1 Method Of Numerical Simulation 16
2.6.2 Results of Numerical Simulation 20
2.7 REPETITION-RATE TUNING OF OSCILLATOR 20
2.8 SYSTEM OVERVIEW 23
3 THz TIME DOMAIN SPECTROMETER 29
3.1 THz GENERATION AND DETECTION 29
3.2 SYSTEM OVERVIEW 31
3.2.1 Detailed Description Of The Spectrometer 31
3.2.2 Data Collection 37
3.3 THEORY AND ANALYSIS 37
4 CHARACTERIZATION OF FIBER LASER AND THz-TDS MEASUREMENTS 41
4.1 OSCILLATOR CHARACTERIZATION 41
4.1.1 Autocorrelation Measurement Of Oscillator Pulse . . 41
4.1.2 Optical Spectrum Of Oscillator 44
4.1.3 Pulse Train Measurements Of Oscillator 45
4.2 AMPLIFIER CHARACTERIZATION 47
4.2.1 Autocorrelation Measurement Of Amplifier System . 47
4.2.2 Optical Spectrum And Power Scaling Measurement . 48
4.3 THz-TDS MEASUREMENTS AT DIFFERENT REPETITION-RATES OF FIBER LASER 50
5 CONCLUSION 55
REFERENCES 59

LIST OF TABLES

TABLES

Table 2.1 Simulator parameters 19

Table 2.2 Calculated OSCAT parameters 23

Table 3.1 Electrical and Optical excitation parameters for PCA [55] 36

LIST OF FIGURES

FIGURES

Figure 1.1 Electromagnetic spectrum [1] 1

Figure 1.2 Loss characteristic of silica based fiber as a function of wavelength [9] 3

Figure 2.1 Basic structure of a fiber 10

Figure 2.2 Illustration of split-step Fourier method used for numerical simulations 17

Figure 2.3 Screenshot of interface of simulation 18

Figure 2.4 The simulation result of pulse duration of the oscillator output . . . 21

Figure 2.5 The simulation result of spectrum of the oscillator output 21

Figure 2.6 Schematic representation of repetition rate tuning [39] 22

Figure 2.7 Schematic representation of Yb-doped fiber laser oscillator 24

Figure 2.8 Yb-doped fiber laser oscillator with fiber and free space lengths . . 24

Figure 2.9 The photo of implemented mode-locked Yb-doped laser oscillator . 26

Figure 2.10 The labeled photo of implemented mode-locked Yb-doped laser oscillator 27

Figure 2.11 Schematic representation of Yb doped fiber laser amplifier 27

Figure 2.12 The photo of implemented pre-amplifier system 28

Figure 2.13 The labeled photo of implemented pre-amplifier system 28

Figure 3.1 a) Side view of PC antenna b) Top view of PC antenna 30

Figure 3.2 THz-TDS system 32

Figure 3.3 The photo of THz-TDs system 33

Figure 3.4 The labeled photo of THz-TDs system 34

Figure 3.5 Dimensions of the PCA-40-05-10 (units are in micrometers) [55] . . 34

Figure 3.6 Photographs of PC antenna a. Front view (laser side) b. Back view (THz side) 35

Figure 4.1 Autocorrelation result of the oscillator output from PBS 43

Figure 4.2 Autocorrelation result of the oscillator output from BS 43

Figure 4.3 Measured spectra obtained from oscillator output 44

Figure 4.4 RF spectra of pulses at different cavity lengths 45

Figure 4.5 Repetition rate at different cavity lengths 46

Figure 4.6 Autocorrelation measurement of amplifier output 47

Figure 4.7 The pulse duration as a function of output power 48

Figure 4.8 Measured spectra obtained from the power amplifier output 49

Figure 4.9 Measured signal power as a function of pump power 49

Figure 4.10 Power stability of the amplifier output 50

Figure 4.11 THz signal for 0 mm oscillator scan stage position 52

Figure 4.12 THz signal for 3 mm oscillator scan stage position 52

Figure 4.13 THz signal for 6 mm oscillator scan stage position 53

Figure 4.14 Power spectra of the THz signals for different scan stage position . 53

LIST OF ABBREVIATIONS

ASOPS	Asynchronous optical sampling
Cr-GaAs	Chromium-doped gallium arsenide
CW	Continues wave
EM	Electromagnetic
EO	Electro-optic
FTIR	Fourier transform infrared
FWHM	Full width at half maximum
GVD	Group velocity dispertion
HRFZ-Si	High resistivity float zone silicon
HWP	Half wave plate
InP	Indium phosphide
LT-GaAs	Low temperature grown gallium arsenide
Nd	Neodmium
NLSE	Nonlinear Schrödinger equation
NPE	Nonlinear polarization evolution
OSA	Optical spectrum analyzer
OSCAT	Optical sampling by cavity tuning
PBS	Polarizing beam splitter
PM	Polarization maintaining
PCA	Photoconductive antenna
PPF	Pump protection filter
QWP	Quarter wave plate
RD-SOS	Radiation damaged silicon on-sapphire
S/N	Signal-to-noise ratio
SA	Saturable absorber
SFM	Self-phase modulation
SPLP	Single-mode pump protection
SRS	Stimulated Raman scattering
TES	Terahertz emission spectroscopy
THz-TDS	Terahertz time domain spectrometer
TRTS	Time resolved terahertz spectroscopy
Tm	Thulium

UFO	Ultrafast Optics Lasers Laboratory
WDM	Wavelength-division multiplexer
WP	Wollaston prism
Yb	Ytterbium

CHAPTER 1

INTRODUCTION

Tera- is a prefix donating multiplication by 10^{12}. Therefore, terahertz is ten to the power twelve hertz. It is also, in physics, specific frequency region in the electromagnetic (EM) spectrum between 10^{11} and 10^{13} Hz. In other words, this range is between microwave and infrared regions. These waves so called T-rays have 4.1 meV energy at 1 THz. 1 THz corresponds to 48 K temperature, 1 ps duration, 300 μm wavelength and 33.3 cm^{-1} wavenumber [1].These values are shown in Figure 1.1.

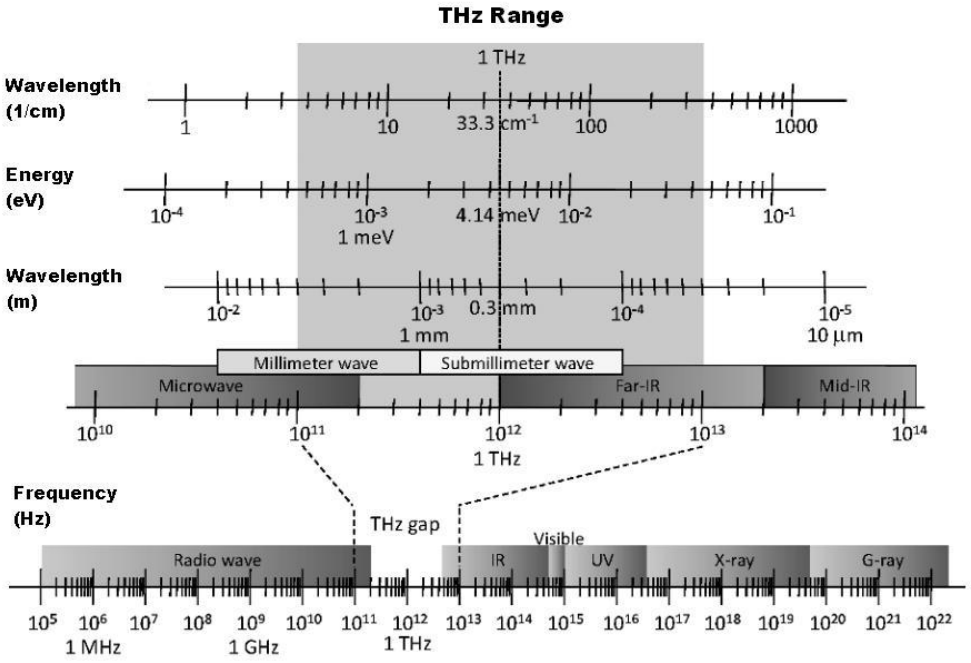

Figure 1.1: Electromagnetic spectrum [1]

Terahertz region is also called as THz Gap as it falls between electronics (longer wave-

lengths) and optics (high frequency) [2]. Consequently, generation and detection systems of THz require combination of these two technologies while THz radiation is not visible to human eye. However, optical rules differ in this region. For example, metals are reflective to THz waves while most dielectrics are transparent. Due to their transparent properties in THz region, some polymers such as Teflon, TPX, and some semi-conductors such as silicon, germanium, and gallium arsenide are commonly used in THz systems. On the other hand, electronic technologies are another necessity of THz experiment setups. Combining these two techniques crates THz radiation sources which can be classified into two groups such as pulsed and continuous wave (CW) radiation [3]. In biology, chemistry, physics and material science, these two techniques have many applications [4]. In addition to these THz sources, THz can be radiated naturally. Due to its incoherent radiation, this naturally occurring THz radiation is not easy to use as radiation source [5].

Although combining optical and electronic technologies is a great challenge, THz region has many unique properties that draw attention worldwide. As can be deduced from unit conversions, T-rays have unique characteristics in EM spectrum which make scientists study this area enthusiastically. One of many, THz waves is sensitive to polar structures in materials. Polarity of materials is highly absorptive the incoming T-rays. Rotational mode in a dipole structured material can be easily detected through THz transmission or reflection spectra. Each material has its own unique response called its finger print and this finger print can be identified via THz waves [2].

Undoubtedly, the most successful of THz applications has been in the development of time-domain terahertz spectroscopic and imaging systems which has been employed in the characterization of dielectrics and semiconductors. This pulsed technique has allowed users to determine characteristics of materials with picosecond resolution.

Scientists in THz wave technologies have benefited from the recent developments in ultrafast laser technologies and RF technologies and applied these new gained techniques into characterizing a wide variety of phenomena. Typically THz-TDS measurements require the use of femtosecond pulses derived from free-space solid state lasers and fiber lasers.

First optical fibers were produced in 1920s [6, 8]. Basic principle which is total internal

reflection have been the same as todays most developed fiber lasers. Pioneer designs had glass-air interface that is sensitive to environmental effects which causes scattering at glass surface. Development of clad at fabrication of fibers in 1950s solved this problem and highly improved the guidance of light through the fiber core [9, 12]. Second mile stone in the development of fiber is production of low loss silica fibers in 1979 [13]. This material that has high level of purity is limited by Rayleigh scattering. The variation of loss in silica with respect to wavelength is displayed in Figure 1.2 and the lowest lost (0.2 dB/km) is achieved at about 1.55 μm which is the reason why this wavelength is used in modern telecommunication systems [14].

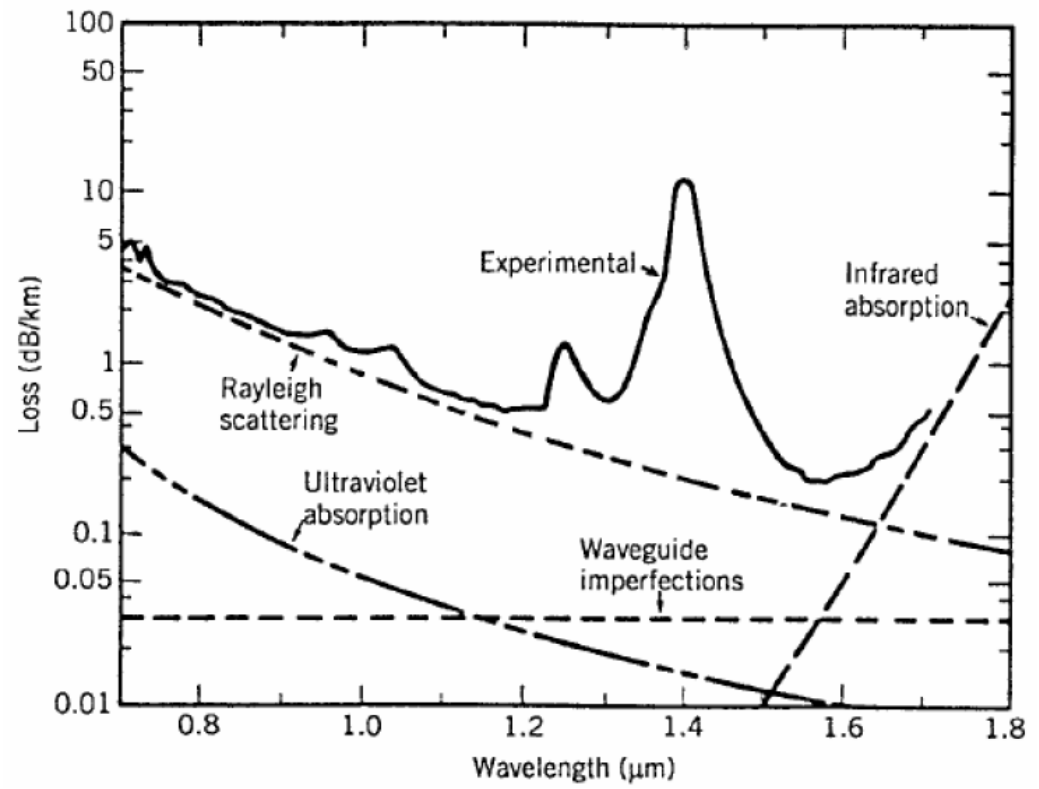

Figure 1.2: Loss characteristic of silica based fiber as a function of wavelength [9]

These major developments gave birth to new phenomena such as nonlinear fiber optics. By forcing intense light into small area of fiber core for long distances, nonlinear effects come to surface. Non-linear effects such as Raman and Brillouin scatterings were studied in 1970s [15, 17]. Next studies were birefringence, parametric four-wave mixing and self-phase modulation [18, 22]. In 1970s, formation of soliton-like pulses were suggested

and by considering the effects of nonlinearity and dispersion were studied [23, 24]. Availability of rare-earth doped (especially Erbium doped) fiber and development of oscillators gave birth to soliton-like mode-locked fiber lasers [25, 26], stretched-pulse (dispersion-managed soliton)[27], similariton [28, 29], all-normal-dispersion (dissipative soliton) [30] and most recently soliton-similariton fiber lasers [31].

To achieve high average power and pulse energy, many amplifier designs were studied. Frontier master-oscillator-power-amplifier design started to appear in 1980s. The limitation of such laser design was that coupling more than ∼1W into core of fiber which has a small area was difficult in order to amplify the incoming signal light. Development of double clad fibers solved this problem by coupling high power into cladding allowing high power pumping [32]. With these developments, today it is possible to achieve 10 kW power level with robust, efficient designs with high beam quality [33].

1.1 TERAHERTZ TIME DOMAIN SPECTROSCOPY

Spectroscopy is used to understand the structure of materials such as semiconductors and bulk materials. The structure determines the response of material to the electromagnetic region that is used in the spectroscopic system. Fundamental work in spectroscopy was done by Czerny in submilimeter wave region where it was to study rotational spectra of HCl in 1925 [34].

Generally, THz spectroscopy can be separated into three main groups such as Terahertz time-domain spectroscopy (THz-TDS) which is mainly studied in this thesis, time resolved terahertz spectroscopy (TRTS) and terahertz emission spectroscopy (TES) [35].

Simply, THz-TDS is generation and probing of THz radiation in the time-domain. Such system has two optical lines: generation and detection lines which are in the same experiment setup. As a source, an ultrafast laser is used and incoming pulse is divided into two arms one of which generates THz radiation. This beam is called the pump beam while other beam detects THz pulse that is called the probe beam. While scanning probe beam with interferometric steps in time domain, THz wave form is obtained as a function of time. This first measurement of THz waveform is used as

reference. Measurement of sample under THz radiation in spectroscopy system is also recorded and called as sample measurement. Comparison of these two measurements under Fourier Transform reveals spectroscopic information about sample. Generally, time-shift of main THz peak is related to refractive index and amplitude change is related to power absorption of sample. This is the result of direct measurement of both phase and amplitude of THz electric filed. Comparing to Fourier transform infrared (FTIR) spectroscopy where only intensity is measured, it is not possible to directly calculate refractive index and extinction coefficient. Additionally, complex permittivity can be calculated without the use of Kramers-Kronig analysis. Another advantage of THz-TDS compared to FTIR is temporal resolution. Temporal resolution of THz-TDS is in order of picoseconds which higher than FTIR spectroscopy [5].

In TRTS which is a time depended operation, sample is excited via photons in third arm. Excitation by laser pulse causes changes in carriers and permittivity of sample can be studied. In other words, dynamic properties of material can be investigated via TRTS compared to THZ-TDS.

Third spectroscopy technique is TES in which the sample itself is the source of THz emission. The THz waveform is analyzed to obtain information about the processes responsible for the emission such as optical rectification, shift currents, and charge transfer. Consequently, motions of high energetic photo excited carriers are investigated and as a result, velocity and momentum changes are studied in TES while evolution of energy is measured in TRTS [35].

With invention of mode-locked femtosecond lasers, scientist have been exploring THz region of electromagnetic spectra as THz spectroscopy experiments [1]. In conventional THz spectroscopy experiments an optical pulse is split into two parts on of which is used to generate and second part is used to as detect arm. Afterwards, transmitted THz signal through sample and detection arm are superimposed on the detection crystal. In order to create temporally delay one pulse with regard to the other, mechanical delay lines are used. These mechanical delays can include linear motorized stages [35], rotating mirrors [36]. Generally, scan speed of these interferometric techniques can last at least tens of minutes with about 100 ps time-window. Rapid scan technique is used to achieve shorter scan durations [37]. However, this method requires external

delay line either which creates about 20 ps time-window. Another technique called as asynchronous optical sampling (ASOPS) provides faster scan times. However, this technique includes two femtosecond lasers which are tuned their repetition rate slightly in synchronization [38]. Consequently, this system requires high stabilization of repetition rates of lasers. Additionally, second femtosecond laser makes a more complex system and increases price of this technique. OSCAT method overcomes this problem as one femtosecond laser source is required [39]. In the first example of this system, Er-doped all fiber design is implemented in THz spectroscopy that do not require free-space propagation and the use of mechanical delay stages. However, these systems lack the energy per pulse due to their inefficient gain medium which limits maximum average power. By using a highly efficient laser gain medium such as Yb-doped fibers, it is possible to achieve energy levels per pulse as traditional solid-state amplified laser sources can. Here we discuss the advantages of a THz spectrometer driven by an ultrafast Yb-doped fiber laser with efficient gain medium of Yb-doped fiber laser and robust operation. Furthermore, the system that we are developing will allow for rapid measurements of THz pulse profiles which will be essential for scanning the entire THz waveform.

1.2 ULTRAFAST FIBER LASERS

Although, there is no generally accepted definition of ultrafast or ultrashort, typically this term means such pulses whose pulse duration is at most a few tens of picoseconds, up to the range of femtoseconds where pico- and femto- stands for 10^{-12} and 10^{-15} respectively as prefixes. This time interval corresponds to a few cycles of harmonic oscillation of the electric field of light with exceptional temporal precision. Additionally, concentration of electromagnetic energy to such short time intervals causes enormous peak powers.

Over last decades, the most used ultrafast lasers were Ti:sapphire. Ti:sapphire are preferred due to their wide bandwidth and superior thermal properties. Although their attractive characteristics, these lasers are expensive, complex and they need external cooling system. An alternative solution has solved this problem. Development of fiber based lasers offers robust, compact and short pulse duration. Use of Er-doped fiber

laser has advantage of telecom-compatible components and it is possible to produce all fiber ultrashort fiber lasers without water cooling systems. Also, other rare earth elements are available to use ultrafast fiber lasers at many other wavelengths. Thulium (Tm), neodymium (Nd) or ytterbium (Yb) can be used to construct mode-locked fiber laser with pulse durations around 30 fs to 1 ns at alternative repetition rates. Combination of direct modulation of continues wave signal and pulse compression stages allow generation of femtosecond pulses [40]. It is also possible to produce ultrafast pulses via gain-switched diode lasers with pulse compression and amplification [41]. Pulses energies from pJ to μJ are achievable with specific amplification techniques. Up to 10 nJ pulse energy can be produced by direct amplification of Raman solitons [42]. Using chirped pulse amplification of chirped pulse systems, this increases up to a few microjoules [43]. This can be further increased by same technique with Yb doped fiber lasers up to mJ regime [44].

Fiber laser systems are more compact, robust and inexpensive. Additionally, rare-earth doped fiber lasers have high saturation energies due to their long relaxation times about ms range. Fibers as flexible guiding medium can be bent to store compactly. Moreover, large area to volume ratio decreases the thermal effects.

Er-doped fiber lasers are commonly used because its operation wavelength 1.55 μm corresponds to telecommunication window. This common use has developed many components for this region such as fibers with both normal and anomalous dispersion. Hence, components are cheaper and more accessible compared to 1 μm. However, Yb doped fibers have better performance due to their efficiencies which enables to produce higher pulse energies.

In this study, we presente a compact THz-TDS driven by a robust Yb-doped fiber laser operating at 51 MHz repletion rate, 1031 nm central wavelength and $\sim$80 fs pulse duration. A parallel line InGaAs based photoconductive antenna was used as THz emitter and a $<$110$>$-cut 2 mm ZnTe crystal was used in electro-optical sampling.

Developments in mode-locked femtosecond lasers have enabled many THz studies to explore THz gap as THz-TDS experiments. In classical THz-TDS systems, time delay between generation and detection arm is scanned by a computer controlled linear stage. This interferometric process is repeated stepwise with integration time of several

hundreds of milliseconds over THz waveform. Therefore, this technique takes more ten minutes. OSCAT technique is proved to achieve about 2 min scan times for about 100 ps time window with an intracavity stepper motor. The main goal of this thesis is to demonstrate that repetition rate tuning of Yb-doped pre-amplified laser system can be used in OSCAT technique for near-real time measurements of terahertz spectrum. In this study, we presented a compact THz-TDS driven by a robust Yb-doped fiber laser operating at about 51 MHz repletion rate, 1031 nm central wavelength and ∼80 fs pulse duration. We demonstrate that repetition rate of Yb-doped laser can be tuned over 50 kHz which can cover about 100 ps time window in OSCAT technique. Afterwards, classical THz-TDS measurements are carried at different repetition rates of fiber oscillator to show stability of system. A parallel line photoconductive antenna was used as THz emitter and a <110>-cut ZnTe crystal was used in electro-optical sampling.

In the second chapter, background on fiber laser including nonlinear optics in fiber, dispersion, pulse propagation in fiber, mode locking theory, system overview and repetition-rate tuning of oscillator are given. Similarly, third chapter explains THz time domain spectrometer with brief explanation of generation and detection techniques, system overview, theory and analysis. Chapter four includes the all experimental work done in this thesis. Finally, chapter five concludes thesis with a summary.

CHAPTER 2

BACKGROUND OF FIBER LASER

Ultra-fast optics is based on mainly dispersion, nonlinearity. Pulse propagation in fiber can be understood by analyzing Maxwell's Equations inside fiber medium. In the first five sub-section of this chapter these phenomenon are explained with mode-locking theory. In next section, simulation of oscillator is given with its methodology. After investigating repetition rate of oscillator, system overview of both oscillator and pre-amplifier is explained. Therefore, this chapter covers full background information about fiber laser systems.

2.1 OPTICAL FIBERS

Fiber structure consists of core, clad, buffer and buffer in modern designs as shown in Figure 2.1. Light mostly travel through core where is placed in the middle of fiber. Among many, simplest fiber design called as step-index fibers have core and clad with uniform refractive index. Cladding has slightly lower index of refraction in order to obtain total internal reflection. These two indexes determine the parameter of numerical aperture (NA). This parameter is related to maximum angle of incidence to guide incoming light through fiber core and calculated as:

$$sin\theta_{max} = NA = (n_1^2 - n_2^2)^{1/2} \tag{2.1}$$

where core with an refractive index of n_1 surrounded by also a glass cladding with index of n_2. Second important parameter of fiber is normalized frequency (V-parameter) which is related to number of modes that an optical fiber can support. It can be

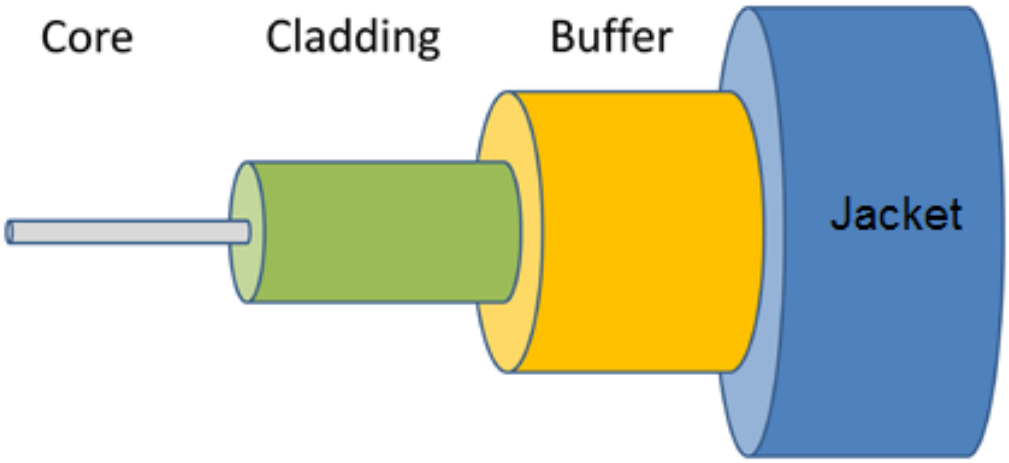

Figure 2.1: Basic structure of a fiber

calculated as:

$$V = k_0 \cdot a \cdot NA \tag{2.2}$$

where wave number is $k_0 = \omega/c = 2\pi/\lambda$, a is core radius. Mainly, this parameter is less than 2.405 for single-mode fiber. For large V values, number of guided modes can be calculated as:

$$M \approx \frac{4}{\pi^2} V^2 \tag{2.3}$$

2.2 DISPERSION

Generally, dispersion is dependency of velocity of light with respect to its frequency. In other words, different wavelengths travel at different velocities in a medium. Dispersion can be classified into three groups as material (or chromatic dispersion), waveguide and modal dispersions. Main contribution comes from the material dispersion which is related to the frequency depended refractive index: $n(\omega)$. This dependency is related to characteristic resonant absorption frequencies of the medium and can be calculated by approximately by Sellmeier equation for frequencies far from resonance frequencies [45]:

$$n^2 = 1 + \sum_{j=1}^{m} \frac{B_j \, \omega_j^2}{\omega_j^2 - \omega^2} \tag{2.4}$$

where ω_j is the resonance frequency and B_j is its strength parameter. To calculate for silica this equation, strength parameters are 0.696, 0.408, 0.897 at resonant wavelengths of 0.0684 μm, 0.116 μm, and 9.896 μm respectively [45]. In common use of silica for wavelength between 0.3 μm and 2.0 μm, there is no resonances.

Ultrashort pulses have a broad range of wavelength and chromatic dispersion gains more importance as pulse duration is shortened. Although material dispersion causes pulse to be broadened, in presence of nonlinear effects it makes mode-locked femtosecond fiber lasers possible. By applying Taylor series to propagation constant, effects of dispersion can be studied at ω_0 where the pulse spectrum is centered [45]:

$$\beta(\omega) = n(\omega)\,\frac{\omega}{c} = \beta_0 + \beta_1\,(\omega - \omega_0) + \frac{1}{2!}\,\beta_2(\omega - \omega_0)^2 + \dots \tag{2.5}$$

where $n(\omega) = n_{eff}(\omega)$ is the effective index of the fiber and $\beta_n = d^n\beta/d\omega^n$. First few terms have special physical significance as [45]:

$$\beta_0 = \frac{1}{c} n(\omega_0)\,\omega_0 \tag{2.6}$$

$$\beta_1 = \frac{1}{c}\left(n(\omega) + \omega\frac{dn(\omega)}{d\omega}\right)_{\omega_0} = \frac{n_g}{c} = \frac{1}{v_g} \tag{2.7}$$

$$\beta_2 = \frac{1}{c}\left(2\frac{dn(\omega)}{d\omega} + \omega\frac{d^2n(\omega)}{d\omega^2}\right)_{\omega_0} \tag{2.8}$$

where c is speed of light, n_g the group is index and v_g is the group velocity. Physically, propagation of envelope of a pulse propagates which is group velocity equals to inverse of β_1 while β_2 represents the dispersion of group velocity. This term is responsible for broadening of the pulse in time. Therefore, β_2 is called as the group velocity dispersion (GVD) parameter.

In optical fiber communications community, commonly the dispersion parameter D is used instead of β_2, which are related to each other by the following equation [45]:

$$D = \frac{d\beta_1}{d\lambda} = -\frac{2\pi c}{\lambda^2}\beta_2 \cong \frac{\lambda}{c}\frac{d^2n(\lambda)}{d\lambda^2} \tag{2.9}$$

where $\lambda = 2\pi c/\omega$ is the wavelength corresponding to the frequency ω.

Waveguide dispersion occurs since the different frequency components in a waveguide have different propagation constants along the propagation direction. Modal dispersion is also similar; different modes in a waveguide have different propagation constants.

This effect is observed in multi-mode fibers. Generally, the effect level of modal dispersion is higher than the waveguide dispersion. However, it does not occur in single-mode fibers.

2.3 NONLINEAR OPTICS IN FIBER

Starting point of nonlinear optics starts from the change of material characteristics in the presence of intense light. Among many, Kerr effect and Raman have essential effect on ultrashort pulses. Kerr effect is an instantaneous influence in mode locked laser while Raman scattering is a delayed effect.

Kerr effect is related to nonlinear contribution the refractive index caused by the incident electric field at frequency, ω. The nonlinear refractive index can be represented as:

$$n = n_0 + \Delta n_{NL} = n_0 + n_2 I \tag{2.10}$$

where n_0 is the linear refractive index and n_2 is an optical constant that determines the strength of the optical nonlinearity. It can be calculated as:

$$n_2 = \frac{3}{8n_0} Re(\chi^{(3)}) \tag{2.11}$$

and where $\chi^{(3)}$ is third order susceptibility. The Kerr coefficient of silica is measured as about $2.7 \cdot 10^{-20}\, m^2/W$ for the wavelengths around $1\,\mu m$ [46].

$$I = n_2 \, |E|^2 \tag{2.12}$$

I is the intensity of the incident field. This process is also known as Kerr nonlinearity which has important outcomes such as self-phase modulation, cross-phase modulation and self-focusing effects. As intensity of light increases, phase delay of light changes with its own intensity. This phenomenon is called as self-phase modulation (SFM) which is modulation is the most important consequence of the Kerr effect for short pulses in fiber. Self-phase modulation with dispersion effect main characteristics of propagation of short pulses in fiber. It creates new frequency components in pulses and causes some frequency chipping while it does not change the envelope of pulse. In presence of dispersion, SFM results in solitonic effect which means maintaining pulse shape while it travels at constant speed.

The dependency of phase delay for light to other beams intensity is called as cross-phase modulation. This effect occurs when there are more than one beams propagating in same medium together with different wavelengths. Self-focusing is dependency of refractive index on the radial distance from center of fiber that caused by intense electric field of light.

Other important phenomenon in nonlinear fiber medium is Raman scattering. This effect is the scattering of photons from optical phonons in fiber namely silica. It can be divided into two categories according to their energy shift with respect to scattering photons. In Stoke Raman scattering energy of incoming photon is absorbed by material and emitted a lower energy as photons. Emitted photons have lower frequency. However, anti-Stoke Raman scattering causes emitted photons with higher energy level because phonons lose their energy after interaction. Intensity ratio between anti-Stokes to Stokes scattering can be calculated as:

$$\frac{I_{anti-Stokes}}{I_{Stokes}} = exp\left(-\hbar\Omega/k_B T\right) \tag{2.13}$$

where $\hbar$ is reduced Planck constant, Ω is the difference between angular frequency of input and output photons, k_B is Boltzmann constant and T is the temperature.

Spontaneous Raman scattering can be stimulated scattering which is called as stimulated Raman scattering (SRS). This effect is dominantly observed with short pulses in fibers. Growth rate of Stokes intensity in propagation direction (z) can be calculated using following formulae [45]:

$$\frac{dI_s}{dz} = g_R I_p I_s \tag{2.14}$$

where I_s is intensity of Stokes beam, I_p is pump beam intensity and g_R is the Raman gain coefficient of medium. Ultrashort pulses with a wide range of wavelength can act as pump beams that cause Raman scattering. This can result in tendency of pulse wavelength to shift longer wavelength. This effect called as self-frequency shift is particularly important for soliton propagation where peak power does not decrease rapidly.

2.4 PULSE PROPAGATION IN FIBER

Maxwell equations are the fundamental tools of electromagnetic phenomena. These equations can be used to derive wave equation with linear and nonlinear induced electric polarization.

$$\nabla^2 E - \frac{1}{c^2}\frac{\partial^2 E}{\partial t^2} = \mu_0 \left(\frac{\partial^2 P_L}{\partial t^2} + \frac{\partial^2 P_{NL}}{\partial t^2} \right) \tag{2.15}$$

where E is electric field of radiation, c is speed of light in vacuum, μ_0 is the vacuum permeability. Equation 2.15 is valid for a nonmagnetic, homogenous medium without free charges like fibers. After several mathematical steps and assumptions, solution of wave equation can be driven as nonlinear Schrödinger equation [45]:

$$\frac{\partial A}{\partial z} + \frac{\alpha}{2}A + \frac{i\beta_2}{2}\frac{\partial^2 A}{\partial T^2} - \frac{\beta_3}{6}\frac{\partial^3 A}{\partial T^3} = i\gamma \left[|A|^2 A + \frac{i}{\omega_0}\frac{\partial(|A|^2 A)}{\partial T} - T_R A \frac{\partial |A|^2}{\partial T} \right] \tag{2.16}$$

where $T = t - \frac{z}{v_g} \equiv t - \beta_1 z$. v_g is group velocity in direction, z. A is the normalized pulse amplitude such that $|A|^2$ gives the optical power of pulses. α is absorption coefficient of medium. β_2 is the second-order group velocity dispersion coefficient. β_3 is third-order dispersion term. γ is the nonlinear parameter which is defined as:

$$\gamma = \frac{n_2(\omega_0)\omega_0}{c\, A_{eff}} \tag{2.17}$$

ω_0 is central frequency. A_{eff} is the effective mode area of an optical fiber and defined in terms of modal distribution function as: If modal distribution is approximated to a Gaussian function, effective area is equal to $\pi\omega^2$. T_R in Equation 2.16 is defined as the first moment of the nonlinear response function $T_R = \int_{-\infty}^{\infty} tR(t)dt$ which is for self-frequency shift. Nonlinear Schrödinger equation is used to model laser and create simulation to comprehend laser oscillators.

2.5 MODE LOCKING THEORY

Generally, mode-locking is to fix phase relations of longitudinal modes of a resonant cavity which is fiber oscillator in this thesis. Number of longitudinal modes (n) with corresponding wavelength (λ_n) is limited by length of cavity (L) by:

$$n\lambda_n = 2L \tag{2.18}$$

When this condition is met, total electric field of all modes can be calculated as:

$$E(z,t) = \sum_n E_n(z,t) = \sum_n E_{0,n} e^{ik_n z - i\omega_n t} \sum_n |E_{0,n}| \, e^{i\phi_n} e^{ik_n z - i\omega_n t} \tag{2.19}$$

where $E_{0,n}$ is the complex amplitude of the n-th mode and ϕ_n its phase. Using Equation 2.19, intensity can be calculated as follows, if all modes are assumed to have same amplitude of E_0 for simplicity.

$$I(z,t) \propto E(z,t)E^*(z,t) = |E_0|^2 \sum_{n=1}^{N} \sum_{m=1}^{N} e^{i(\phi_n - \phi_m)} (m-n)\Omega \left(\frac{z}{c} - t\right) \tag{2.20}$$

where Ω is the frequency difference between two successive modes.

$$\Omega = \omega_{n+1} - \omega_n = \frac{\pi c}{L} \tag{2.21}$$

If mode locking condition is satisfied, Equation 2.20 is further simplified to;

$$I(z,t) \propto E(z,t)E^*(z,t) = |E_0|^2 \, e^{i\delta\phi} \sum_{n=1}^{N} \sum_{m=1}^{N} e^{i(m-n)\Omega(z/c-t)} \tag{2.22}$$

where phase relations between longitudinal modes are fixed. The second exponential part in the above equation will be 1 for all terms of the sum if the condition:

$$\Omega \left(\frac{z}{c} - t\right) = 2\pi j \tag{2.23}$$

where j is integer. When this condition is achieved, maximum intensity is proportional to square of number of modes.

$$I_{max} = N^2 \, |E_0|^2 \equiv N^2 I_0 \tag{2.24}$$

Using Equation 2.23, temporal and spatial distances of adjacent pulses as:

$$\Delta z = 2L; \;\; \Delta t = 2L/c \equiv T \tag{2.25}$$

Equation 2.25 means that the maximum intensity is repeated with the round trip time T of the laser resonator. Full width at half maximum (FWHM) of the pulses can be calculated, the N modes is assumed to be interfere as planar waves at a fixed time, $t = 0$. Using geometric series, Equation 2.22 becomes:

$$I(t) = I_0 \frac{sin^2(\frac{N\Omega}{2}t)}{sin^2(\frac{\Omega}{2}t)} \tag{2.26}$$

Consequently, the FWHM of the pulses can be derived from the Equation 2.26 as:

$$I(\Delta T) = \frac{1}{2} I_{max}; \;\; \Delta T = \frac{1}{N} \frac{2L}{c} = \frac{1}{N} T \tag{2.27}$$

According to Equation 2.26, the pulse width is shortened as the number of superposed modes increases. It is directly proportional to the revolution time of the laser cavity.

Another technique is to achieve mode locking is modulating the gain of the cavity with the difference frequency Ω of subsequent modes. This results in additional time dependence of the electromagnetic field in the cavity as:

$$\begin{aligned} E_n(z,t) &= (E_{0,n} + E_n^{mod} cos\,\Omega t) e^{ik_n z - i\omega_n t} \\ &= \left[E_{0,n} e^{-i\omega_n t} + \frac{1}{2} E_n^{mod} (e^{-i\Omega t} + e^{i\Omega t} e^{-i\omega_n t} \right] e^{ik_n z} \\ &= \left[E_{0,n} e^{-i\omega_n t} + \frac{1}{2} E_n^{mod} (e^{-i\omega_{n+1} t} + e^{-i\omega_{n-1} t}) \right] e^{ik_n z} \end{aligned} \tag{2.28}$$

According to Equation 2.26, each mode induces sidebands and frequency of these sidebands overlaps with the ones of consecutive modes. This condition is valid for total bandwidth that results in mode locking.

Mode locking conditions can be achieved by mainly two methods as active and passive mode locking. While modulation by acoustic-optic and electro-optic modulators are used in active mode locking, saturable absorbers nonlinear polarization evolution technique can be used to achieve passive mode locking.

2.6 NUMERICAL SIMULATIONS OF OSCILLATOR

Before constructing Yb-doped fiber oscillator, a 50 MHz oscillator is simulated using simulation software which is developed by Ultrafast Optics & Lasers Laboratory (UFO) in Bilkent University. In this section background of this software is given with the output results.

2.6.1 Method Of Numerical Simulation

Using the split-step Fourier method to solve nonlinear Schrödinger equation (NLSE), pulse propagation of pulses is simulated. In this method, it is assumed that dispersion and nonlinear effects act independently over a short distance of fiber medium. Effects of second and third-order dispersion, linear losses, saturable gain and nonlinear effects such as gain dispersion, Raman scattering, self-phase modulation, saturable absorption

and band-pass filter many of which is explained in this chapter are included in the simulation software. Input pulse can be assumed to be noise or Gaussian profile. These effects are applied to oscillating pulse at each round trip. NLSE with all of these effects is shown in Equation 2.16. This equation can be expressed in terms of operators as:

$$\frac{\partial A}{\partial z} = \left(\widehat{D} + \widehat{N}\right) A \tag{2.29}$$

where $\widehat{D}$ is the differential operator including dispersion and absorption in a linear medium and $\widehat{W}$ is the nonlinear operator with all nonlinear effects on pulse propagation. These two operators are given as:

$$\widehat{D} = \frac{\alpha}{2} A + \frac{i\beta_2}{2} \frac{\partial^2 A}{\partial T^2} - \frac{\beta_3}{6} \frac{\partial^3 A}{\partial T^3} \tag{2.30}$$

$$\widehat{N} = i\gamma \left[|A|^2 A + \frac{i}{\omega_0} \frac{\partial (|A|^2 A)}{\partial T} - T_R A \frac{\partial |A|^2}{\partial T} \right] \tag{2.31}$$

In this method, distance traveled is divided into h sub-distances. In first and second halves, only dispersion effects the pulse propagation. In the mid-section effects of nonlinearity are include. This process is displayed in Figure 2.2

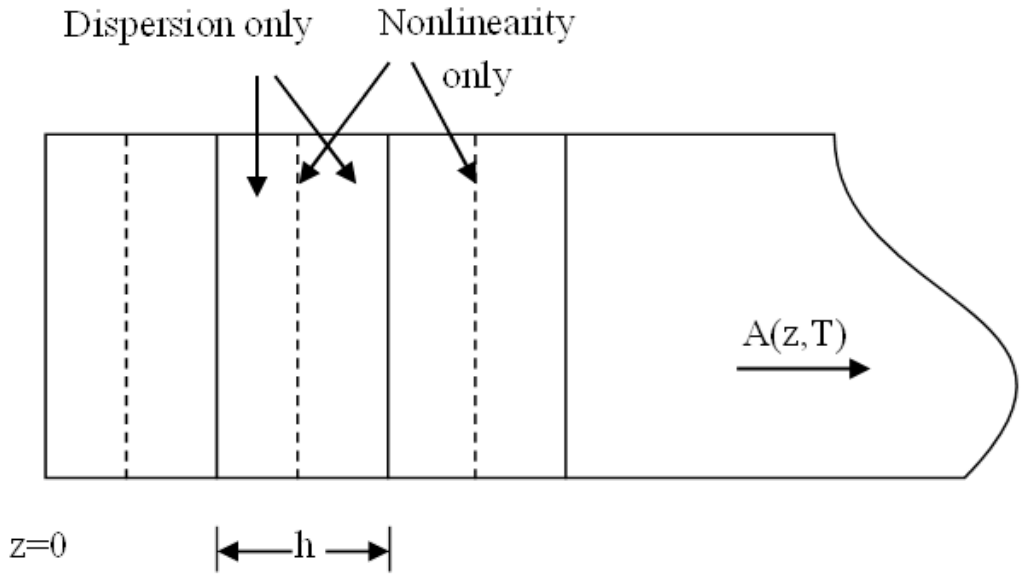

Figure 2.2: Illustration of split-step Fourier method used for numerical simulations

Mathematically,

$$A\left(z+h,T\right) \approx exp\left(\frac{h}{2}\widehat{D}\right) exp\left(\int_{z}^{z+h} \widehat{N}\left(z'\right) dz'\right) exp\left(\frac{h}{2}\widehat{D}\right) A\left(z,T\right) \tag{2.32}$$

In Fourier domain, this term becomes:

$$exp\left(\frac{h}{2}\widehat{D}\right) A\left(z,\tau\right) = F_T^{-1} exp\left(\frac{h}{2}\widehat{D}\left(i\omega\right)\right) F_T A(z,\tau) \tag{2.33}$$

where F_T denotes the Fourier transform operation. $\widehat{D}\left(i\omega\right)$ is just a number in the Fourier space. Therefore, the evaluation of Equation 2.32 becomes straightforward.

A screenshot of interface of simulation is shown in Figure 2.3

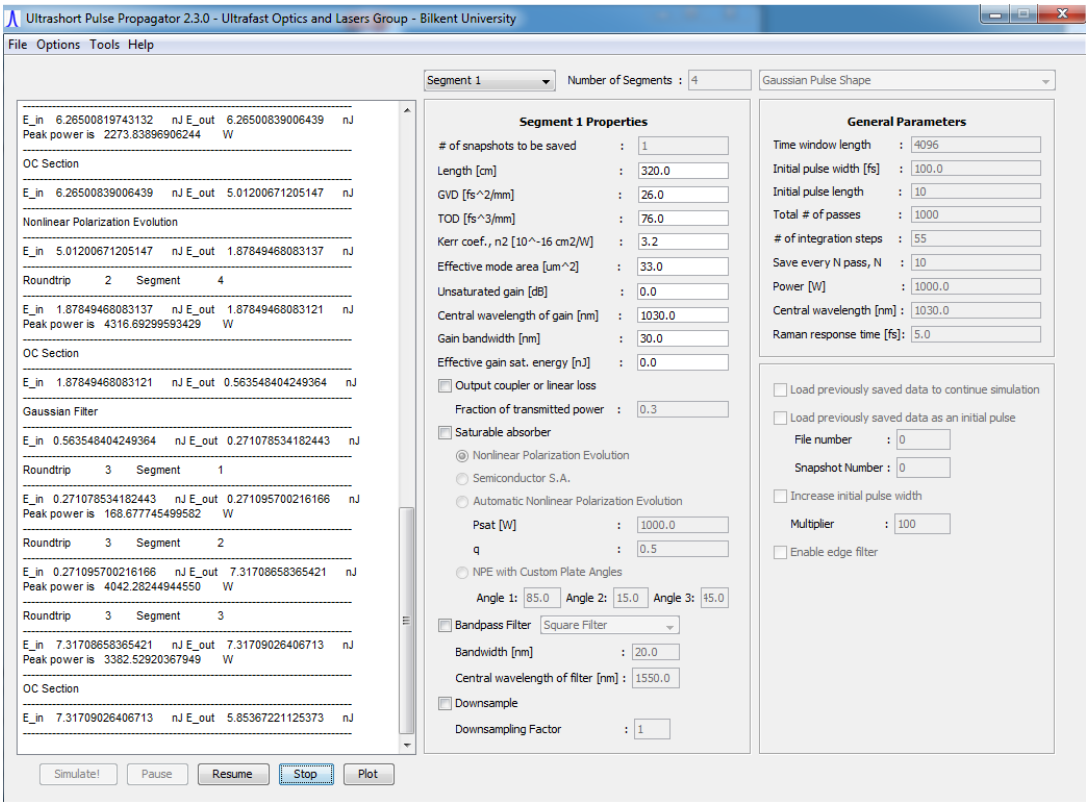

Figure 2.3: Screenshot of interface of simulation

The parameters to be entered into the simulator are listed in Table 2.1

Simulation is divided into sub-section that has the unique characteristics such as fiber, gratings, NPE etc. The saturable absorber (SA) process is included in a specific segment by an amplitude modulation. The total nonlinear phase shift stored over

Table2.1: Simulator parameters

Parameter	Function
Time window length	Number of data points for discretizing time
Initial pulse width $[fs]$	Actual length of the pulse corresponding to a number of data points
Initial pulse length	Number of discrete points representing the FWHM of initial pulse
Total number of passes	Number of passes to be made over the entire sequence of segments
Number of integration steps	Number of discrete steps taken per each page per segment
Save every N pass, N	Number of round trips after which data is saved to file
Power $[W]$	Actual power corresponding to unit size of power
Central wavelength $[nm]$	The central wavelength of the light used for simulation
Raman response time $[fs]$	Parameter characterizing the strength of the Raman effect
Number of snapshots to be saved	Number of segments each fiber section is divided into
Length $[cm]$	Physical length of the segment
GVD $[fs^2/mm]$	Second order dispersion parameter
TOD $[fs^3/mm]$	Third order dispersion parameter
Kerr coef., n2 $[10^{-16}cm^2/W]$	The Kerr nonlinearity coefficient
Effective mode area $[\mu m^2]$	Effective mode area for the propagating beam
Unsaturated gain $[dB]$	Small signal gain of the amplifier
Gain bandwidth $[nm]$	Finite gain bandwidth for parabolic approximation
Effective gain sat. energy	Saturation energy in arbitrary units for the gain
Output coupler /linear loss	Adds an output coupler to the end of the segment

the each round trip is converted into this amplitude modulation which is modeled for semiconductor and NPE in the simulation as:

$$I_{SSA} = 1 - \frac{q}{1 + I/I_{sat}} \tag{2.34}$$

$$I_{NPE} = 1 - q \cdot cos^2\left(\frac{\pi}{2}\frac{I}{I_{sat}}\right) \tag{2.35}$$

where I_{SSA} and I are the intensities before and after SA, q is the modulation depth and I_{sat} is the saturation intensity of the SA. Gain saturation is also taken into account as:

$$g(E) = \frac{g}{1 + \frac{1}{E_{sat}} \int |a|^2 \, d\tau} \tag{2.36}$$

2.6.2 Results of Numerical Simulation

Simulation studies help us to understand the dynamics in laser oscillator. In this power, simulation results of oscillator that produces pulses are given in terms of pulse duration and spectrum. Some important parameters can be given as: $\beta_2 = 26fs^2/mm$, $\beta_3 = 76fs^3/mm$, $n_2 = 3.2 \cdot 10^{-16}cm^2/W$, effective mode area 14.4 and $33.0\mu m^2$ for gain fiber and single mode fiber, $g_0 = 30.0dB$ and effective saturation energy is $2.0nJ$. According to these parameters, oscillator output simulation results are given in Figure 2.4 and 2.5:

According to simulation, Yb-doped fiber oscillator delivers $1.07ps$ pulses at central wavelength of $1031nm$ with $53nm$ bandwidth.

2.7 REPETITION-RATE TUNING OF OSCILLATOR

Femtosecond fiber lasers with a variable delay line are used in many fields such as tomography [47], coherent control [48], and terahertz time-domain spectroscopy [49]. A new technique enables scientist to conduct experiments without external scan lines. Optical sampling by cavity tuning technique is able to tune repetition rate of laser source in order to create a time delay between two outputs of laser with different optical lengths as shown in Figure 2.6 [39]. After pulse i is divided into two arms,

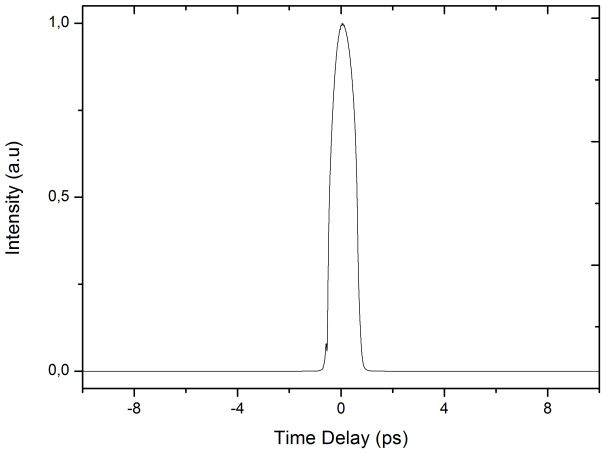

Figure 2.4: The simulation result of pulse duration of the oscillator output

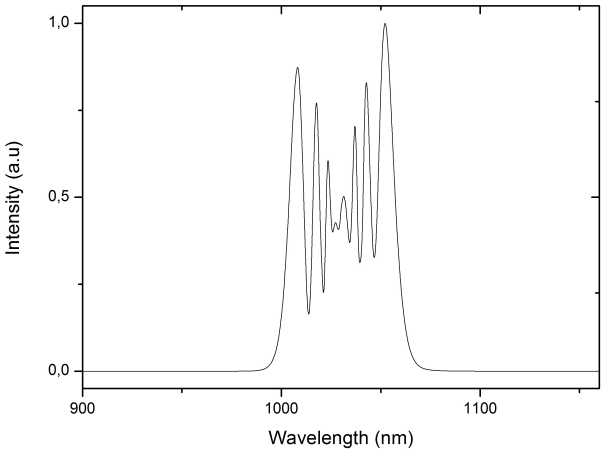

Figure 2.5: The simulation result of spectrum of the oscillator output

pulses in second path travel an extra path length of l_d in time, t_d. In order to create a time delay of Δt between paths, repetition rate of laser is tuned and second arm is shifted more with respect to first arm. However, this technique is developed with

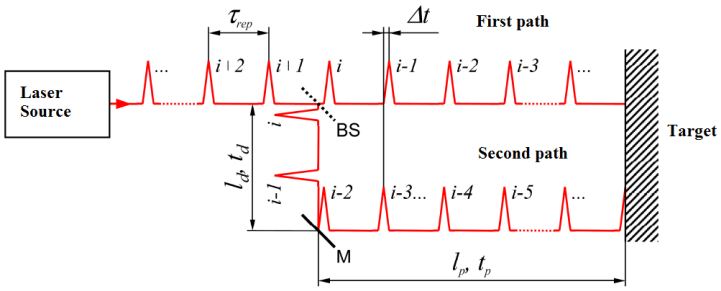

Figure 2.6: Schematic representation of repetition rate tuning [39]

an Erbium doped fiber laser which has an inefficient gain medium compared to Yb doped fiber laser. In this thesis, repetition-rate tuning of Yb doped fiber oscillator is oscillator is studied. Theoretical analysis is same in both cases. Assume that second path has more pulses as number of a at repetition rate of f_{rep}. Time delay between pulses in first path i and second path $i + a$ is given by:

$$\Delta t = t_d - a \cdot \tau_{rep} \tag{2.37}$$

where $\tau_{rep} = \frac{1}{f_{rep}}$. Desired total time scan rage can be calculated as:

$$\Delta t_{range} = \Delta t_{max} - \Delta t_{min} = a \cdot \left(\frac{1}{f_{min}} - \frac{1}{f_{max}} \right) \tag{2.38}$$

where minimum and maximum scanned repetition rates scanned, f_{min},f_{max} respectively. Corresponding length difference for desired scan range can be calculated with pulse number a as:

$$l_d = \frac{a \cdot c_0}{f_{min} \cdot n} \tag{2.39}$$

where c_0 is speed of light and n is refractive index of medium pulses are guided in. According to Equation 2.39, scan range of time depends on, repetition rate of laser, laser tuning range and length of passive delay line. According to these formulas, calculated OSCAT parameters of Yb-doped fiber laser oscillator are given as:

Table2.2: Calculated OSCAT parameters

$f_{REP}(MHz)$	50
$\Delta f(kHz)$	50
$\Delta\tau(ps)$	100
Step size (ps)	0.1
Cavity length (m)	6
Scan length (mm)	6
Pulse index (i)	5,005
$l_{fiber}(m)$	20,02

2.8 SYSTEM OVERVIEW

Yb doped fiber laser system consists of mainly two parts such as passively mode locked laser oscillator and one stage amplifier. Mode locking technique of oscillator used in this thesis is based on nonlinear polarization evolution (NPE) method. Briefly, polarization of the intense center of the pulse is rotated and favored more than the less intense off-center. In detail, pulses from oscillator port of polarizing beam splitter (PBS) are linearly polarized. After passing quarter wave plate, pulses are slightly linearly polarized. In fiber section, polarization of the pulse center will differ from the polarization of the wings due to intensity difference between them. This phenomenon is called as Kerr effect. Polarization filtering mechanism consisting of a second quarter wave plate and half wave plate eliminates the wings of pulse. Center of pulse is transmitted through oscillator by PBS while wings are reflected out. Overall, NPE technique consisting of two quarter wave plate, one half wave plate and a PBS acts as artificial saturable absorber.

In Figure 2.7, diagram of fiber laser oscillator is displayed. Two main coupled equations can be solved with two variables to determine total fiber and free space lengths. Here, variables are grating distance and total fiber length d and x respectively.

$$\frac{x}{\upsilon} + \frac{2d}{c_0} + \frac{l}{c_0} = \frac{1}{f_{rep}} \tag{2.40}$$

$$a \cdot x + b \cdot d = 0 \tag{2.41}$$

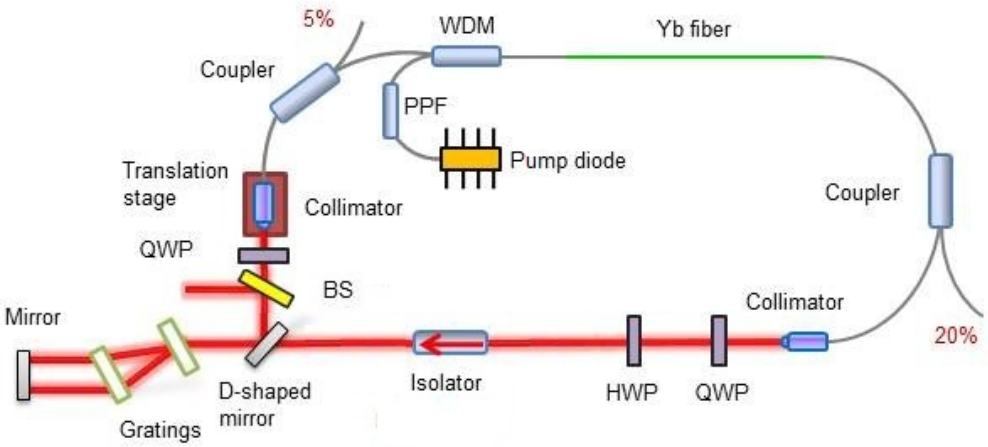

Figure 2.7: Schematic representation of Yb-doped fiber laser oscillator

where v is speed of light inside fiber, l is distance between free space components, a and b is dispersion parameters of fiber and gratings respectively. These calculation leads to a fiber oscillator with corresponding length shown in Figure 2.8:

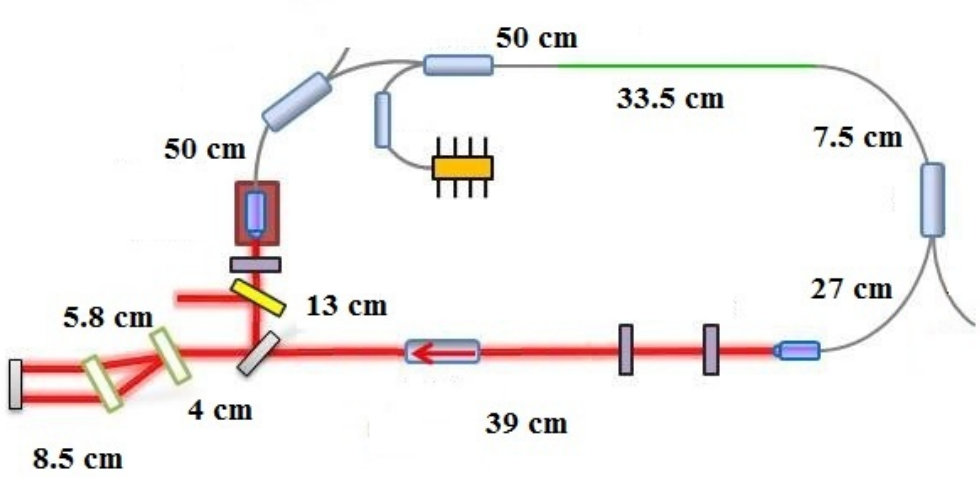

Figure 2.8: Yb-doped fiber laser oscillator with fiber and free space lengths

Fiber and free space components are listed as following:

1. Laser diode operating at 976 nm
2. Single-mode pump protection (SPLP) or pump protection filter (PPF)

3. Wavelength-division multiplexer (WDM)
4. Highly Yb-doped gain fiber
5. Coupler 80/20
6. Collimator x2
7. Quarter wave plate x2
8. Half wave plate x2
9. Bulk isolator
10. D-shaped mirror
11. A pair of gratings
12. Mirror
13. Non polarizing beam splitter cube 50-50
14. Translation stage
15. Coupler 95/5

Implementation of oscillator starts with characterization of fiber-coupled laser diode. To prevent possible damages caused by back reflection in system, laser diode is protected via SPLP. WDM couples the pump and oscillating signal through the highly Yb doped gain fiber whose core diameter is 4 μm. Active fiber has numerical aperture (NA) of 0.14, and absorption 1200 dB/m at 976 nm pump wavelength. Fiber coupled coupler of 80/20 is an optional output to construct a power amplifier arm. Free space starting with collimator includes wave plates as NPE components.

Traditionally, an additional PBS is required to obtain NPE. However, acceptance polarization of bulk isolator is horizontal; i.e it transmits only horizontal polarization as PBS. Additionally, bulk isolator makes system to operate only in one direction. Transmission gratings are used to add negative dispersion to pulses that have positive dispersion due to chromatic dispersion in fiber. A BS cube output is used to couple signal to amplifier part. Second collimator couples free space light into fiber. This

collimator is placed on a translation stage that is used to tune repetition rate. A 95/5 coupler spliced to WDM is used to monitor power and spectrum of oscillator.

The photo of the mode-locked Yb-doped fiber laser oscillator is displayed in Figure 2.9 and 2.10.

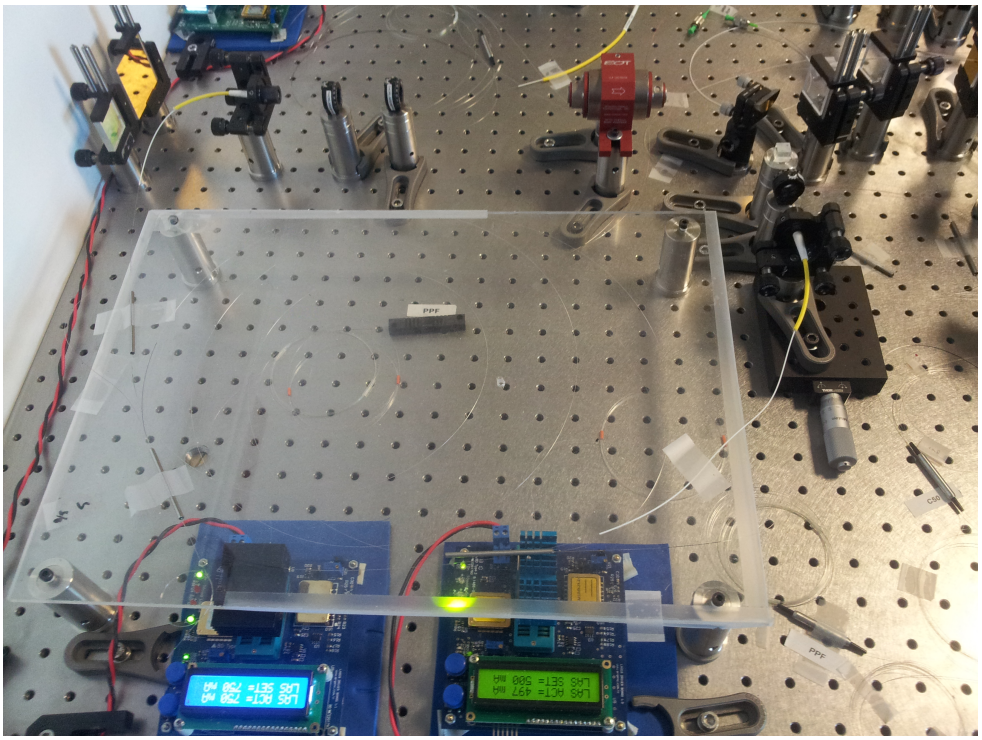

Figure 2.9: The photo of implemented mode-locked Yb-doped laser oscillator

In Figure 2.11, diagram of Yb doped fiber laser amplifier system is shown.

Components of amplifier system are listed as follows:

1. Polarization maintaining (PM) collimator x2
2. PM coupler
3. Laser diode operating at 976 nm
4. Pump protection filter (PPF)
5. PM wavelength-division multiplexer (WDM)
6. PM Yb-doped gain fiber

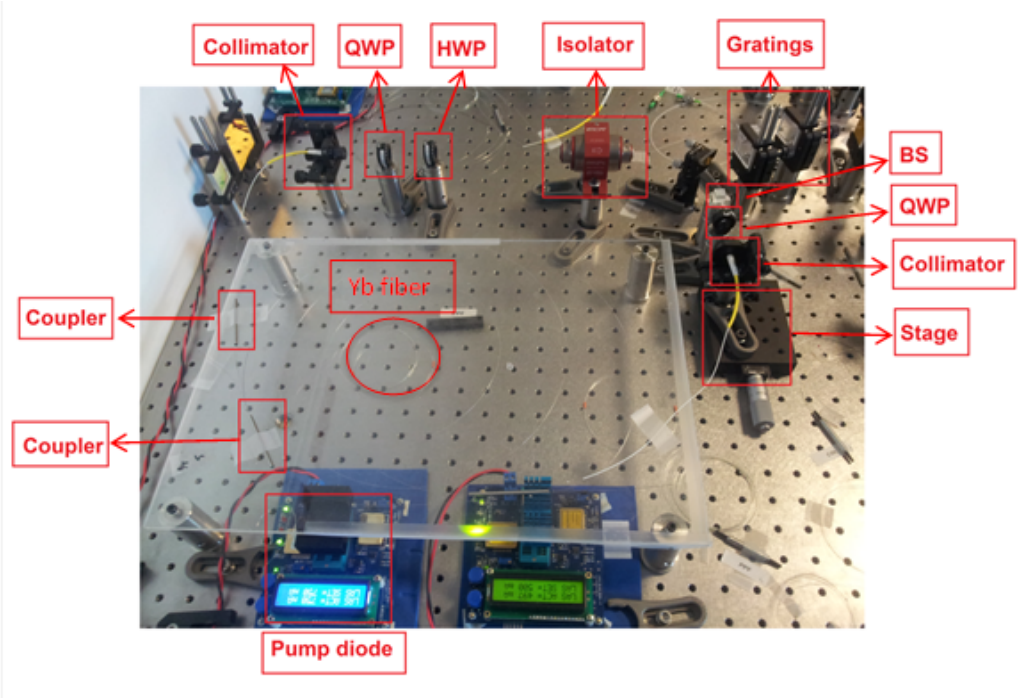

Figure 2.10: The labeled photo of implemented mode-locked Yb-doped laser oscillator

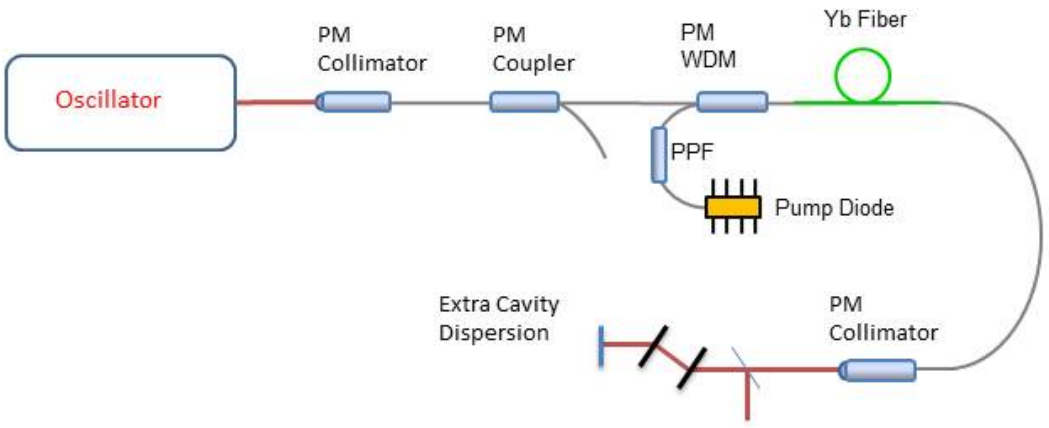

Figure 2.11: Schematic representation of Yb doped fiber laser amplifier

7. A pair of gratings (Volume phase holographic gratings)

8. Mirror x2

BS output of oscillator is coupled to amplifier part via a PM collimator. Vertical polarization of input signal is maintained until the output of amplifier. Output pulses from PM collimator out are compressed with a grating pair. The photo of the pre-amplifier system for laser is displayed in Figure 2.12 and 2.13.

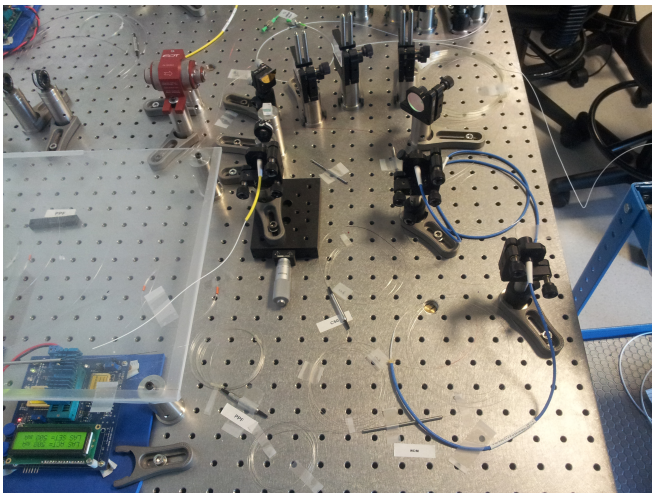

Figure 2.12: The photo of implemented pre-amplifier system

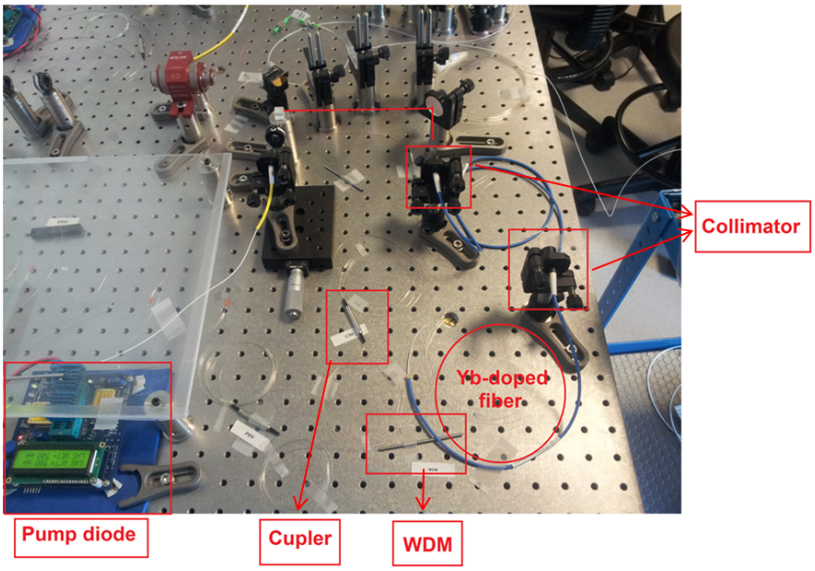

Figure 2.13: The labeled photo of implemented pre-amplifier system

CHAPTER 3

THz TIME DOMAIN SPECTROMETER

THz-TDS has proven to be one of the most productive tools in the far-infrared region over the past two decades. While its unique features allow characterization studies with ultra-fast lasers such as Ti:Al_2O_3 systems operating near 800 nm are used in THz generation and detection in these methods. Developing fiber laser technology enables us to produce ultrafast and powerful pulses that can be used in THz generation systems. Yb-doped fiber laser have greater potential in power scalability and robustness [50]. These ultrafast lasers with sub-200 femtosecond pulses enable scientists to use antenna structures, optical rectification, or surface emitters to produce THz [37]. In detection part, recent studies showed that GaP is an appropriate crystal for electro-optical detection near 1 μm region.

In this thesis, PCA generation and electro-optic (EO) detection techniques will be explained in details although there are other methodologies to generate and detect THz radiation.

3.1 THz GENERATION AND DETECTION

Basically, photo conductive antenna structure contains metal electrodes on semiconductor substrate and a hemispherical lens to converge T-ray into setup. Metal electrodes form an antenna structure with a gap in between them and this structure is shown in Figure 3.1.

In order to generate THz radiation through PCA, a bias voltage is applied to metal electrodes on substrate. Femtosecond pulses from ultrafast laser source are focused on

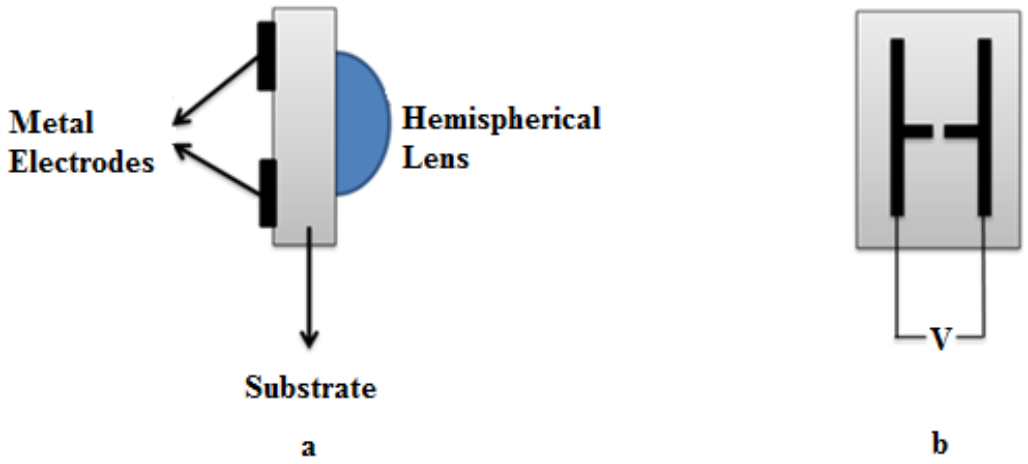

Figure 3.1: a) Side view of PC antenna b) Top view of PC antenna

substrate between gaps of electrodes. This excitation crates electron hole-pairs in the conduction band of substrate that are later accelerated by bias voltage on electrodes. Accelerated electrons result a photo current in dipole which is function of time, $J(t)$. Finally, EM radiation in THz range is emitted proportional to the derivative of this photo current and can be calculated from Hertzian dipole antenna as:

$$E(r,t) = \frac{l_e}{4\pi\epsilon_0 c^2 r}\frac{\partial J(t)}{\partial t} sin\,\theta \propto \frac{J(t)}{\partial t} \tag{3.1}$$

where l_e is the effective length of dipole structure, ϵ_0 is vacuum dielectric constant, c is velocity of light in vacuum, θ is the angle between direction of dipole and emission, r is the distance from dipole [3].

Since, electric field of THz radiation is proportional to time derivative of photo current, faster change of this current results in stronger radiation. This is the reason why femtosecond pulses are obligatory for THz generation. Generated THz pulses have pulse duration in picosecond time range. Carrier mobility and carrier life time of the substrate are crucial characteristics of PCA. Several antenna designs are developed to improve THz generation. Some examples are stripline, dipole, offset dipole, and bowtie antenna structure.

Numerous types of semiconductor substrate can be used to fabricate PCAs such as Low temperature grown gallium arsenide (LT-GaAs), radiation damaged silicon–on-sapphire (RD-SOS), chromium-doped gallium arsenide (Cr-GaAs), indium phosphide

(InP) among which LT-GaAs with shortest carrier life time of 0.3 ps and RD-SOS are most commonly used [1].

In electro-optical sampling, mainly measurement of THz pulse based on phase modulation. Optical pulse propagating through EO crystal with THz pulse experiences a phase modulation. The strength of this modulation is directly proportional to electric field of THz pulse. Electric field of THz crates birefringence in EO crystal that changes the polarization of optical pulse [51]. Change of optical pulse polarization generally is in elliptical state that consists of major and minor components. These components are measured by photodiodes or a balanced photodiode. By analyzing polarization of this pulse using ellipsometry technique, indirectly THz pulse shape can be deduced [52].

There are some limitations for this technique such as pulse duration of optical pulse, second order susceptibility of the photo detector medium. Phase matching condition should be obtained for optical and THz pulse in EO crystal [53, 54]

3.2 SYSTEM OVERVIEW

In this section, a THz-TDS system was explained. This spectrometer contains PCA as THz generator and EO method for detection technique. Therefore, it can be called as antenna-crystal system. THz-TDS is driven by a Yb-doped fiber laser operating at 51 MHz repletion rate, 1031 nm central wavelength and ∼80 fs pulse duration. A parallel line PCA is used as THz generation source and a <110>-cut 2 mm ZnTe crystal.

3.2.1 Detailed Description Of The Spectrometer

Schematic representation of THz-TDS system is shown in Figure 3.2. Ultrashort pulses from Yb-doped fiber laser are divided into two optical arms consisting of generation (pump) and detection (probe) arms. Both arms start from the beam splitter and end at EO crystal. Optical distances between these two components for both arms are equal to each other. Generation arm consists of BS, M2-M5, OL, PCA, FG, P1 and P2. BS, DL, M6, L form probe arm. ZnTe, M7, QWP, WP, BD and lock-in amplifier were used for data collection and data were recorded by computer.

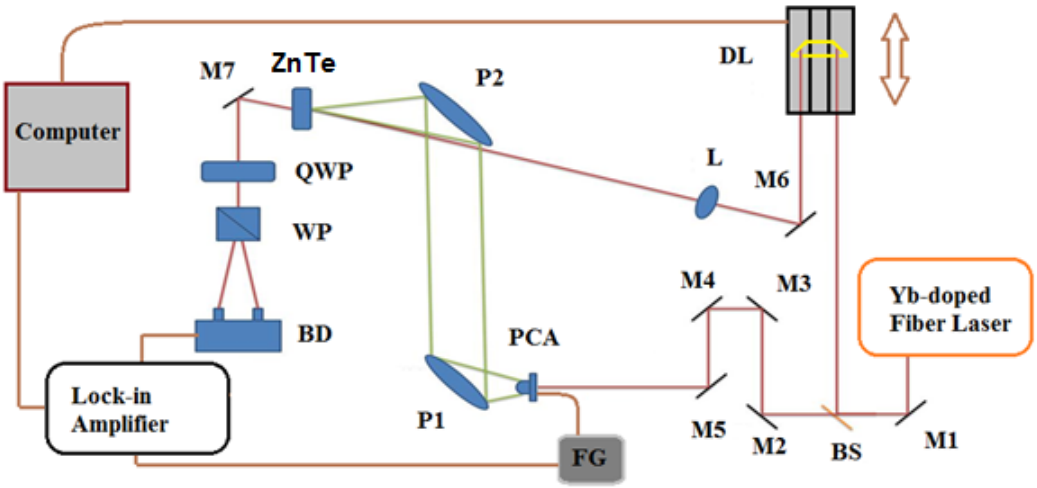

Figure 3.2: THz-TDS system

Components in Figure 3.2 are listed as follows:

1. Yb-doped fiber laser: Home-build, 90 mW, ~80fs, 1031 nm
2. M6: Mirror
3. BS: Beam splitter

   Generation arm
4. M2-M5: Mirrors
5. PCA: Batop PCA-40-05-10-1060-h antenna
6. FG: Function generator
7. P1-P2: Off-axis parabolic mirrors

   Detection arm
8. DL: Delay line consisting of corner cube on translation stage
9. M6: Mirror
10. L: Lens with focal length 300 mm

11. <110> cut ZnTe crystal

Data collection components

12. M7: Mirror
13. QWP: Achromatic quarter wave plate for 700-1100 nm
14. WP: Wollaston prism
15. BD: New Focus 2307 balanced photo receiver
16. Lock-in amplifier: Stanford Research System SR830 Lock-in Amplifier [57]
17. Computer

The photo of the pre-amplifier system for laser is displayed in Figure 3.3 and 3.4.

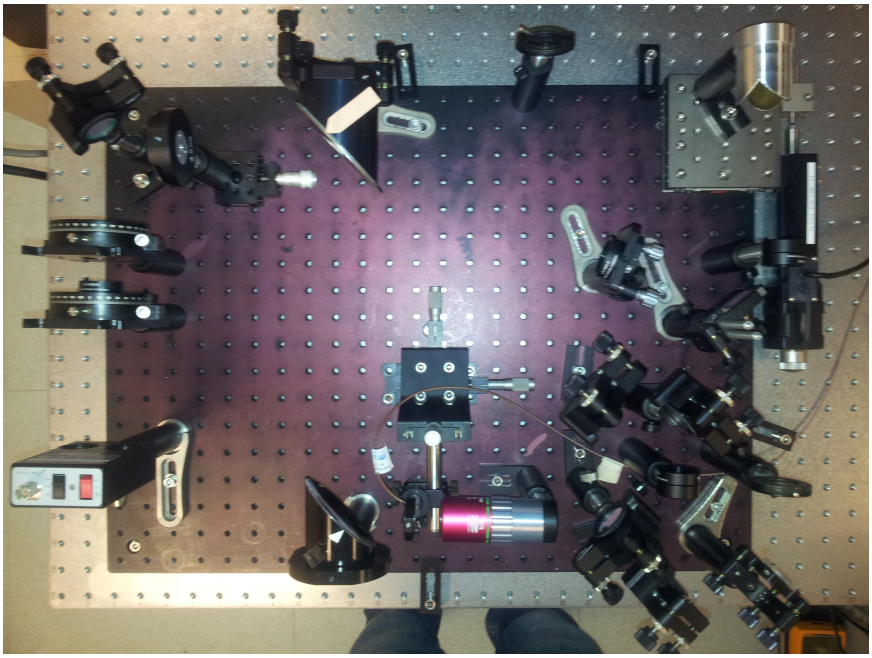

Figure 3.3: The photo of THz-TDs system

Yb-doped fiber laser delivers over 90 mW power. Pulse duration of pulses is ∼80 fs at repetition rate of 51 MHz.

Beam splitter divides ultrashort pulses into two arms such as generation and detection arms. In order to equate the optic baths of both arms M2-M5 mirrors are used as in

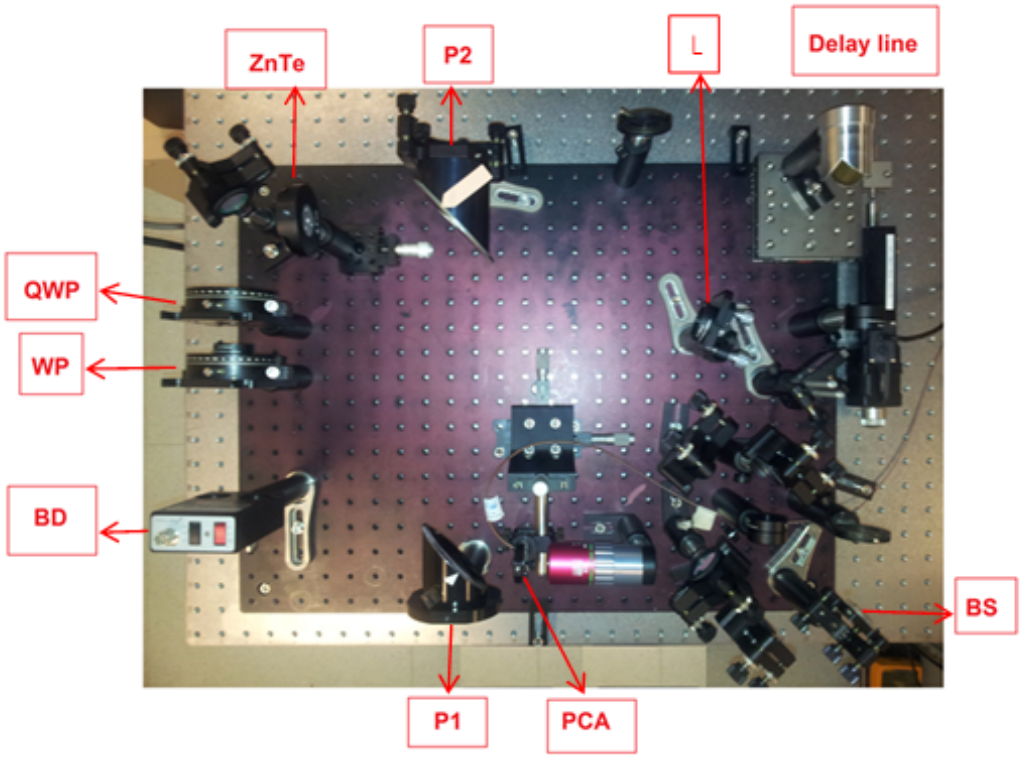

Figure 3.4: The labeled photo of THz-TDs system

Figure 3.2. Dipole structure antenna with a coupled lens is used in this setup as an emitter. Manufacturer, Batop used LT-InGaAs as semiconductor substrate in antenna structure. Dimensions of PCA are shown in Figure 3.5.

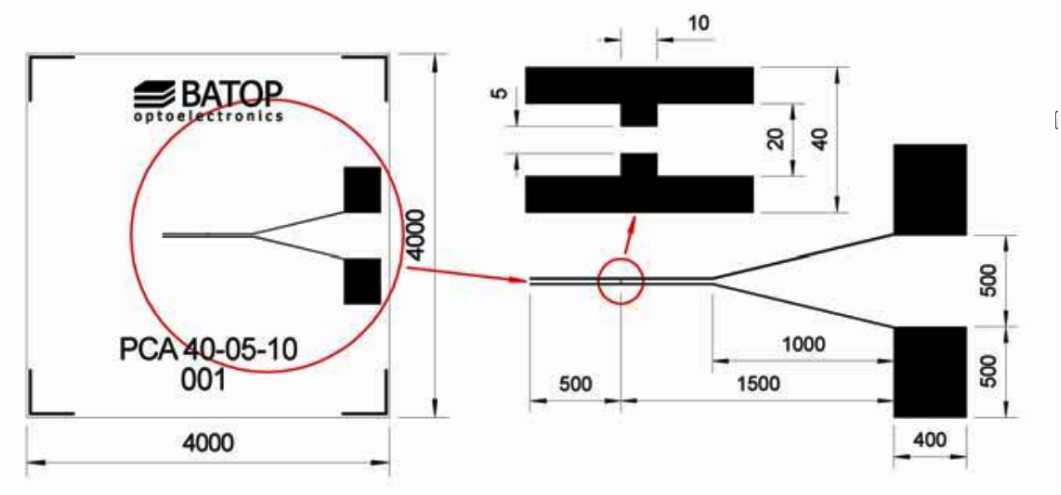

Figure 3.5: Dimensions of the PCA-40-05-10 (units are in micrometers) [55]

Length of the antenna is 40 μm, width of the antenna is 10 μm and the gap between the electrodes is 5 μm (see Figure 3.5) Pulses from laser should be focused on 5 μm gap. Generally an objective lens is used for this purpose. In our case, a focusing lens is already coupled in the antenna structure which makes it is easier to align. The electrodes along with the substrate form a rectangular chip as shown in Figure 3.6a. After this chip, hyper-hemispherical silicon lens made of high resistivity float zone silicon (HRFZ-Si) is placed in order to guide THz beams through the system. This material is the most commonly used material in the THz range due to its frequency independent and high transmission. Structure of the antenna can be seen in Figure 3.6 [55].

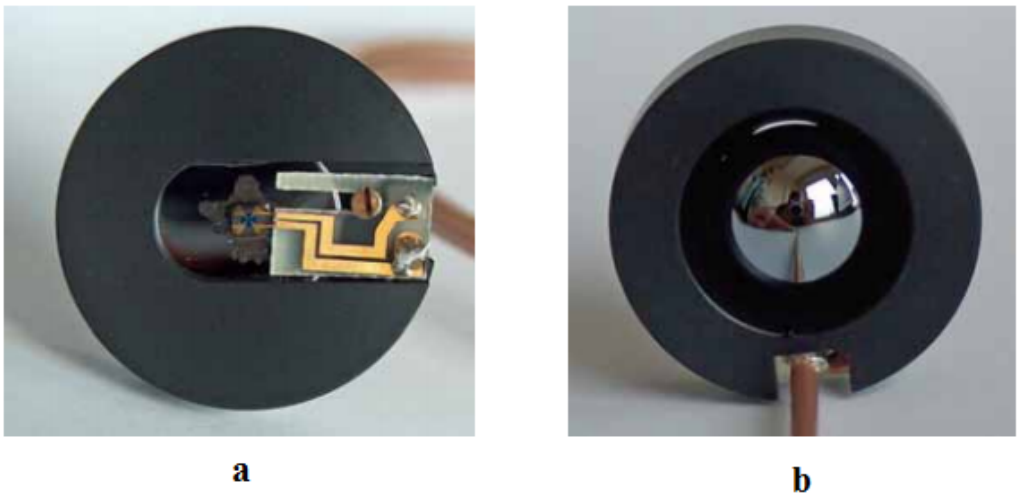

Figure 3.6: Photographs of PC antenna a. Front view (laser side) b. Back view (THz side)

PCA is placed on a xyz stage to align with respect to both parabolic mirror and mostly optical beam. For best alignment of PCA, the resistance of antenna should be minimum at maximum illumination of laser beam onto electrode gap. Additionally, power of light should be kept under a certain level not to damage structure of antenna. These parameters are shown in Table 3.1.

A function generator is used to apply 15 V sinusoidal wave with 1 kHz to antenna for accelerating the electron-hole pairs in the gap. Another output of function generator is connected to lock-in amplifier to synchronize the measurement as reference. Instead of applying an alternating voltage, one can apply a DC voltage with an additional

Table3.1: Electrical and Optical excitation parameters for PCA [55]

Electrical Parameters	
	Standard Ratings
Dark resistance	55 MΩ
Voltage	15 V

Optical Excitation Parameters	
	Standard Ratings
Excitation laser wavelength	1060 nm
Optical mean power	20 mW

optical chopper.

Diverging THz beam from hemispherical silicon lens is collimated via an off-axis parabolic mirror (P1 in Figure 3.2). Then beams are focused by a second parabolic mirror (P2 in Figure 3.2) onto the ZnTe crystal. Parabolic mirrors have focal length of 50.4 mm and 119.4 mm, respectively. They are made of electro-formed nickel[56].

In detection arm, some portion of incoming ultrashort pulses are reflected by beam splitter and directed to gold coated corner cube. Corner cube with a maximum 38 mm reflection distance is placed on a motorized stage (DL, see Figure 3.2). That delay line is controlled by computer with a Labview interface. Using this stage, path difference between generation and detection arm is scanned with precision. After delay line, optical beam is focused on ZnTe by a 300 mm focusing lens (L, see Figure3.2). Although, the angle between generation and THz beams decrease the interaction length of beams through EO crystal, by focusing both beam and careful alignment, it is possible to observe the interaction.

After ZnTe crystal, another mirror is used to align optical beam to quarter wave plate (QWP, see Figure 3.2) which is used to change the polarization of light from elliptical to linear state with an angle that determines the difference between major and minor components of polarization. Then these components are separated by Wollaston prism (WP, see Figure 3.2) with an angle. A balanced photo receiver which is connected to lock-in amplifier measures the difference in vertical and horizontal components.

Using lock-in amplifier, it is possible to detect both voltage and current in nano scale

range. This device locks the reference signal coming from function generator and records only change in this frequency [56].

Information from translation stage and lock-in amplifier is gathered in a computer and THz waveform is obtained in the Labview interface for further analysis.

3.2.2 Data Collection

Detailed description of THz-TDS system used in this thesis is explained in previous section. Computer collects data from lock-in amplifier that is in sync with function generated and controls the translation stage in delay line. Communication between stage and computer is sustained by a stage driver. A Labview program enables to control step size and scan distance of translation stage. Total scan distance of stage is scanned step by step. Generally, these measurements are carried with 10 or 20 μm step sizes. At each step, stage is delayed as time duration of data collection which is the time interval between two consequent steps. This increases the synchronization of stage and lock-in amplifier as well as signal-to-noise ratio. These parameters determine the total time of the THz measurement. Voltage value from lock-in amplifier is recorded and plotter in the time scale as THz wave profile. In next step, data from interface can be used to analyze sample which will be explained in next section. General results are the THz profile in time domain and Fourier transform of THz pulse which is power spectrum of temporal waveform.

3.3 THEORY AND ANALYSIS

In analysis part, Fourier transform is an essential tool to investigate the results of THz-TDS measurements. Direct measurement of polarization change of detection pulse caused by THz electric field helps to relate THz waveform in time domain. This time depended data can be converted into frequency domain via Fourier transform. Consequently, frequency depended analysis give further information. This transform can be calculated as:

$$E(\omega) \equiv A(\omega)e^{-i\phi(\omega)} = \int dt E(t)e^{-i\omega t} \tag{3.2}$$

where $A(\omega)$ is the amplitude of frequency depended electric field and $\phi(\omega)$ phase of this electric field. This transformation provides information about both amplitude and phase of electric field. Then phase and amplitude data can be used to directly calculate absorption coefficient and refractive index of sample which is one of the great advantages of THz-TDS measurements.

Maximum bandwidth of measurement can be calculated from delay time which is related to step size of scan. Optical beam travels 300 μm in 1 ps. Inverse of time interval two between consequent measurements is equal to sampling rate, f_s. Spectral range stars from$-f_s/2$ and ends at $+f_s/2$ with a central frequency, $f_s = 0$. In measurement part, two measurements are necessary; one without sample (with sample holder or air) and one with sample. THz wave through sample vary in amplitude and time. When a sample is placed in THz generation arm, resulting THz wave is delayed due to higher refractive index of refraction in sample. Additionally, THz waves can interact with the molecules in sample resulting in absorption of THz pulses. It is important to measure both cases starting from same scan point because of correct phase shift calculation. After data is recorded, Fourier transform is applied to both reference and sample measurement results. By comparing phase difference and power ratio of both reference and sample Fourier transform, refractive index and absorption coefficient of sample can be calculated, respectively.

Real and imaginary parts of refractive index can be calculated as follow:

$$\tilde{n} = n_r(\omega) + i n_i(\omega) \tag{3.3}$$

where $n_r(\omega)$ is real and $n_i(\omega)$ imaginary parts of refractive index. These components in vacuum can be calculated by using data from THz-TDS measurements as:

$$n_r(\omega) = \frac{1}{kl}\left(\phi\left(\omega, l\right) - \phi\left(\omega\right)\right) \tag{3.4}$$

$$n_i(\omega) = \frac{1}{kl}\left(ln\left(\frac{E\left(\omega, l\right)}{E\left(\omega\right)}\right)\right) \tag{3.5}$$

where k is the wave vector, l is the thickness of sample and $\phi(\omega)$ is the phase of reference measurement. Real part equals to refractive index and imaginary part gives the absorption coefficient. If measurement are carried in air medium real part should be corrected as follow:

$$n_r(\omega) = 1 + \frac{1}{kl}\left(\phi\left(\omega, l\right) - \phi\left(\omega\right)\right) \tag{3.6}$$

Additionally, the power absorption coefficient of the sample is calculating by analyzing the transmission for varying thickness, assuming the measurements are performed in the linear absorption regime [58].

$$n = 1 + c\frac{\Delta t}{l} \tag{3.7}$$

$$\Delta t = \frac{\Delta\phi(\omega)}{2\pi\omega} \tag{3.8}$$

$$n = 1 + \frac{\Delta\phi(\omega)c}{2\pi\omega c} \tag{3.9}$$

$$\alpha = -\frac{1}{l}ln\left(T\right) = \frac{4\pi v n_i\left(\omega\right)}{c} \tag{3.10}$$

Here, n is refractive index, c is speed of light, Δt is time shift, α is absorption coefficient, and T is transmittance.

CHAPTER 4

CHARACTERIZATION OF FIBER LASER AND THz-TDS MEASUREMENTS

In this thesis, a fiber laser oscillator and amplifier were constructed. The system results are discussed in this chapter. Next, terahertz time domain spectrometer driven by this Yb doped fiber laser is studied. In the first part of this chapter, the seed laser namely oscillator will be described, the second part includes amplification system and final part will be about THz-TDS measurements.

4.1 OSCILLATOR CHARACTERIZATION

4.1.1 Autocorrelation Measurement Of Oscillator Pulse

Electronically, it is no possible to measure femtosecond pulse durations because oscilloscopes and photo detectors do not have bandwidths on the order of a few hundred THz. Autocorrelation technique has been developed to characterize pulse duration of femtosecond pulses. This technique is performed in the time domain using nonlinear optical effects. Time domain pulse can be studied by interferometric or intensity autocorrelation. In this thesis intensity autocorrelation is used. Temporal measurements of the pulses are observed by an oscillator and electronic pulse duration is related to femtosecond pulse duration by a correction ratio.

A deconvolution factor is used in Equation 4.1 assuming pulse shape has Gaussian distribution [59].

$$\Delta\tau_{pulse}^{FWHM} = 0.707 \cdot \Delta\tau_{autocorrelation}^{FWHM} \tag{4.1}$$

Traditionally, two QWP, one HWP and a PBS are used to achieve mode-locking condition by NPE technique. As mentioned in Chapter 2, PBS eliminates the less intense off-center wavelengths by rejecting the vertical polarization of oscillation beams. Generally, this output is used for amplification in pre-amplifier part. However, shorter pulse durations can be achieved by using another free space output from oscillator. Using non polarizing beam splitter right after transmission gratings, shorter pulse widths are possible with respect to PBS output. After gratings, pulses become negatively chirped due to angular dispersion and coupled through the fiber by collimator. Material dispersion of silica causes pulses to be positively chirped. This cycle achieves a certain point at which pulses can be compressed to shortest possible pulse duration. This region corresponds to after the gain medium of oscillator. When pre-amplifier design mimics the oscillator design (gratings-Yb-fiber region) including components and fiber length, BS output from oscillator delivers most compressible pulses to pre-amplifier. Additionally, PBS is extracted from system because bulk isolator is functional only for horizontal polarization. In other words, it rejects vertical polarization like PBS.

System improvement can be understood by comparing pulse width of former output (PBS) and new main output (BS) of fiber oscillator displayed in Figure 4.1 and Figure 4.2. For autocorrelation measurements of both oscillator and pre-amplifier outputs, Femtochrome FR-103MN Rapid Scanning Autocorrelator is used in this study.

With correction factor, pulse duration at FWHM is 1.2 ps and 1.09 ps for PBS and BS respectively. The pulse distribution is assumed to be a Gaussian. According to this result, BS produces shorter pulse duration with respect to PBS. With a specific pre-amplifier design, shortest pulses can be achieved by this Yb-doped fiber oscillator. Pulses from BS were seeded the amplifier stage and subsequently was compressed before being used in the THz-TDS system as shown in Figure 2.11.

Simulation results of autocorrelation showed that oscillator delivers 1.07 ps pulses from output. Experimental results verify this theoretical value.

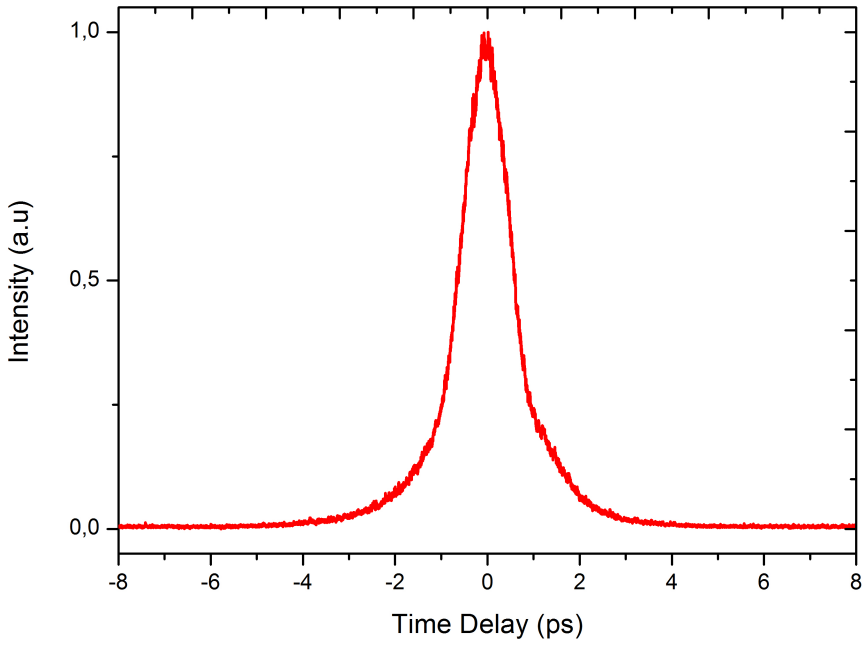

Figure 4.1: Autocorrelation result of the oscillator output from PBS

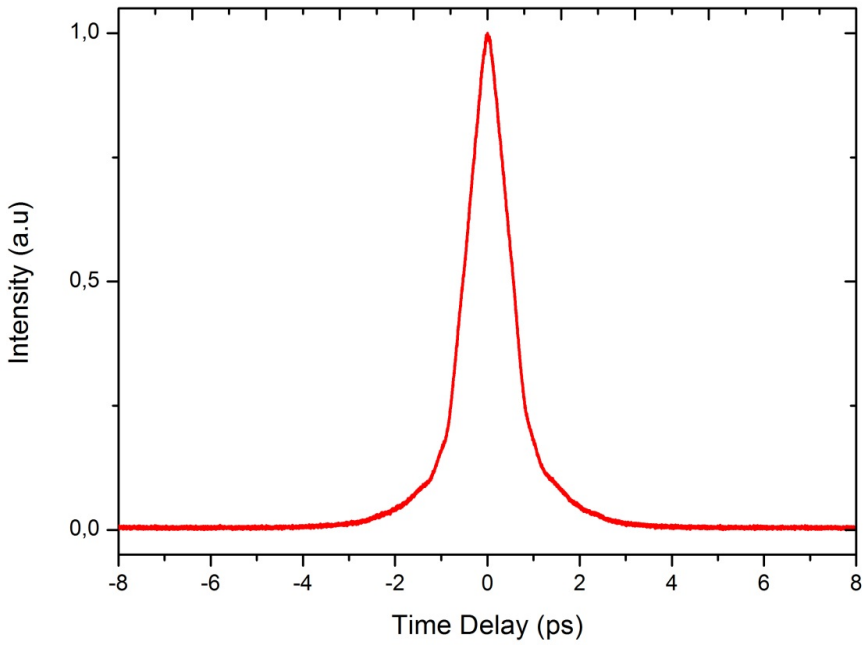

Figure 4.2: Autocorrelation result of the oscillator output from BS

4.1.2 Optical Spectrum Of Oscillator

If the cavity stores too much energy, multiple-pulsing might occur. To confirm energy of laser is split into 50 MHz pulses, multiple-pulsing should be avoided. This can be observed in spectrum or pulse train measurements. In spectra measurement, multiple-pulsing causes a periodic oscillation at every part of spectrum. Spectrum of both oscillator and per-amplifier outputs are measured with Anritsu Optical Spectrum Analyzer (OSA)-MS9740A. In Figure 4.3, a partial oscillation with varying periodicity can be seen which is caused by dispersive effects.

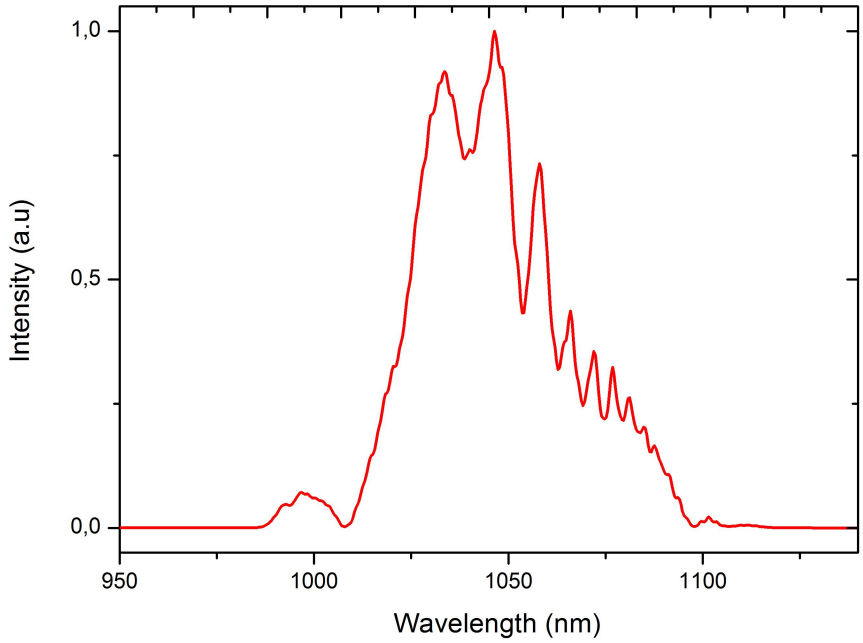

Figure 4.3: Measured spectra obtained from oscillator output

Central wavelength of spectra is 1042 nm and it has 35 nm of bandwidth at FWHM. According to simulation results, spectral bandwidth of oscillator output should be over 50 nm. However, collimator coupling ratio and directionality of collimator affects this result.

4.1.3 Pulse Train Measurements Of Oscillator

The Yb-doped fiber oscillator as shown in Figure 2.3 produces 15 mW of power at about 51 MHz repetition rate from BS output. Central wavelength of oscillator is about 1040 nm 100 fs pulses were derived from 5 % output port at which pulse train measurements are carried. To implement the system in scheme as shown in Figure 3.2, the stability of the oscillator was examined over the entire THz scan length by scanning the collimator over the range of 6 mm. The measured repetition rate with RF analyzer in frequency domain is plotted in Figure 4.4.

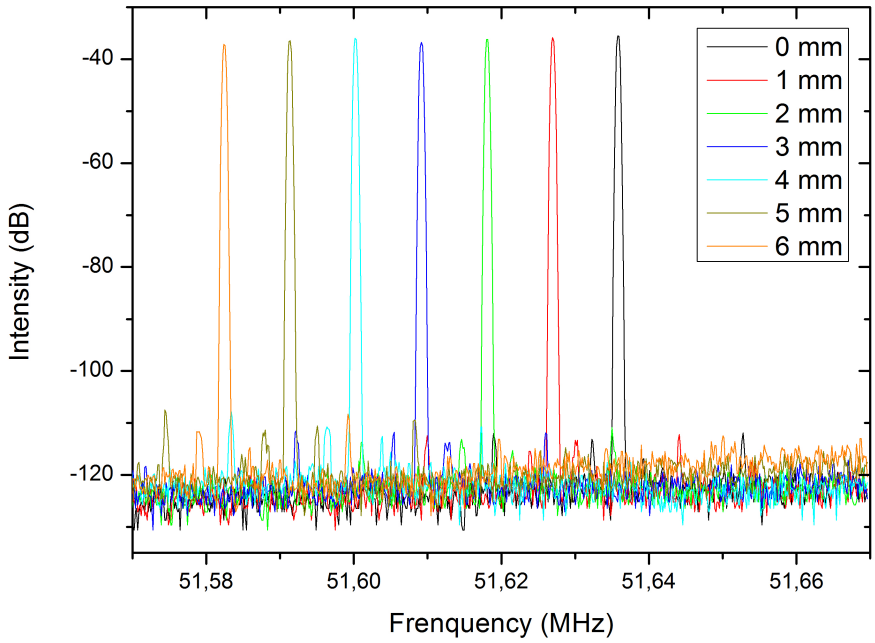

Figure 4.4: RF spectra of pulses at different cavity lengths

From starting point to 6 mm cavity position, prepetition rate is tuned 53.4 kHz over 51.58 MHz. The estimated change was 50 kHz over 50 MHz. Cavity length consisting of fiber optics and free space part was not exactly as calculated. Therefore, there is a difference between theoretical and measured prepetition rate tuning range about 6 %. Another reason that can cause this change is using manual translation stage. Small error in micrometer adjustment can produce larger repetition rate shift. For OSCAT

technique, this change can be compensated by adjusting the scan step length and size. For 1000 data point, instead of scanning 6 mm with 6 μm steps at 50 MHz, THz profile can be measured by shorter scan length for 53.4 kHz because scan length is inversely proportional to repetition rate (Equation 2.39). Additionally, according to results, pulses have about 80 dB suppression ratio which is another stability parameter.

Repetition rate results in Figure 4.4 are transformed into another graph to observe the linear change of frequency of pulses.

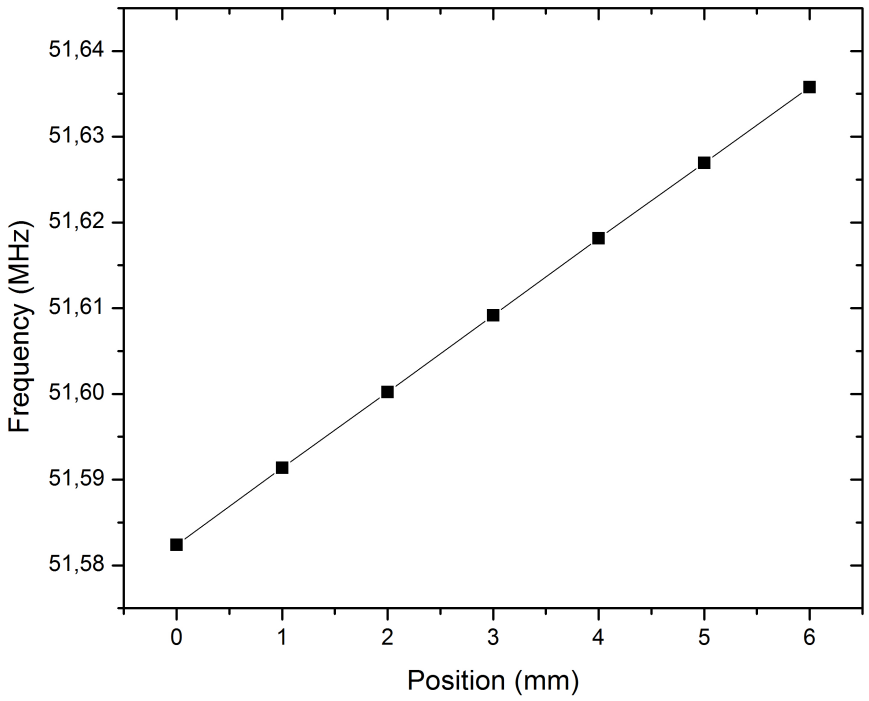

Figure 4.5: Repetition rate at different cavity lengths

According to Figure 4.5, for 6 mm scan rage with 1 mm steps, repetition rate of 51.58 MHz is tuned about 8.9 kHz at each step linearly.

4.2 AMPLIFIER CHARACTERIZATION

4.2.1 Autocorrelation Measurement Of Amplifier System

Pulse durations for scan points are also measured as oscillator scan 6 mm of cavity length. The autocorrelation measurement result of the pulses at 90 mW of average power at different repetition is shown in Figure 4.6. Intensity of output signals are normalized to one.

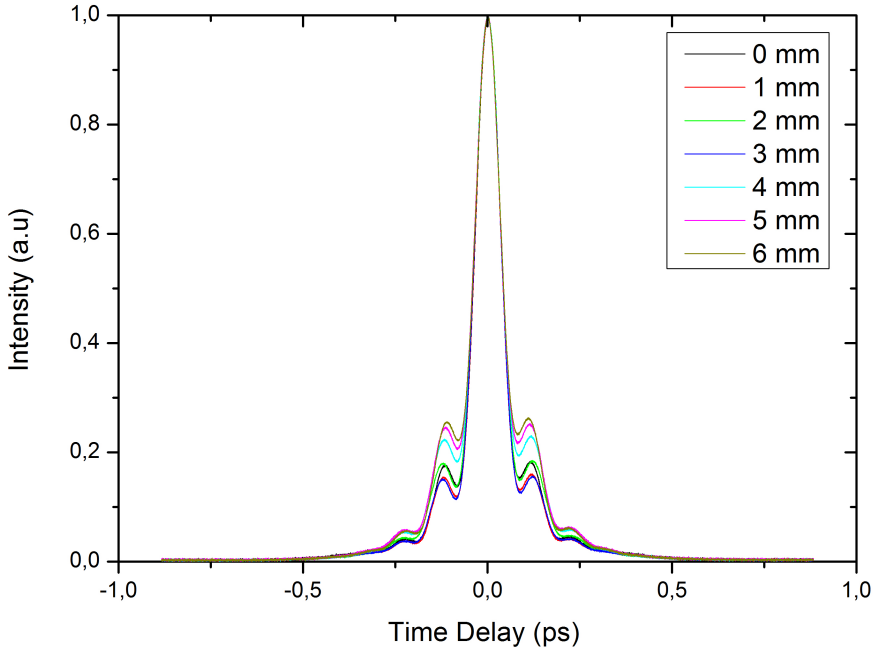

Figure 4.6: Autocorrelation measurement of amplifier output

Although there is some change first and final position, the overall stability of the system is quite good with respect to expected measurements in the THz-TDS system. The pulse width change is below 4 % and measured pulse durations of first and last positions are 85.0 fs and 81.8 fs respectively assuming pulse shapes are Gaussian.

Additionally, variation of pulse duration was measured with different output power of pre-amplifier. Pulse duration for various output power is shown in Figure 4.7. Pulse duration decreases up to certain point due to gain narrowing. At higher power, central

wavelength of highly chirped pulses is amplified with respect to off-center wavelengths, in our case 1031 nm. Therefore, pulse width becomes shorter.

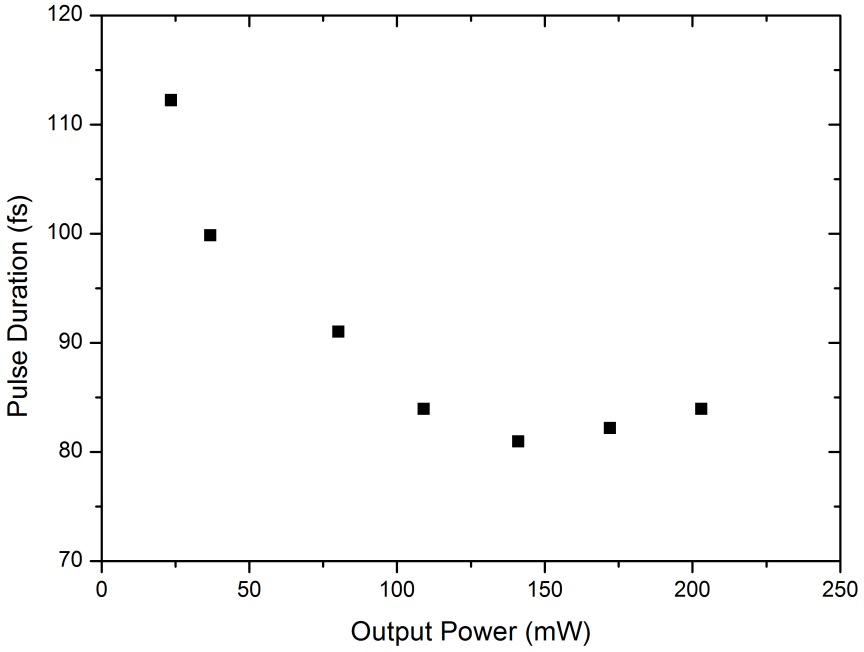

Figure 4.7: The pulse duration as a function of output power

4.2.2 Optical Spectrum And Power Scaling Measurement

In order to observe stability of laser, amplifier output spectra were recorded during the scan interval. The obtained spectra show that the output has a center wavelength of about 1031 nm with a FWHM of 30 nm as shown in Figure 4.8. Spectrum was observed to be stable with changing cavity length.

Power characterization of amplifier includes the measurement of signal power as a function of pump power. Over 200 mW average power is measured at pump power of about 400 mW. According to experimental results, conversion efficiency is calculated to be about 65 %. This efficiency value differs between low and high pump power simply due to the shift of peak emission wavelength of diode.

In Figure 4.10, measured amplifier power is shown while cavity length is tuned. This

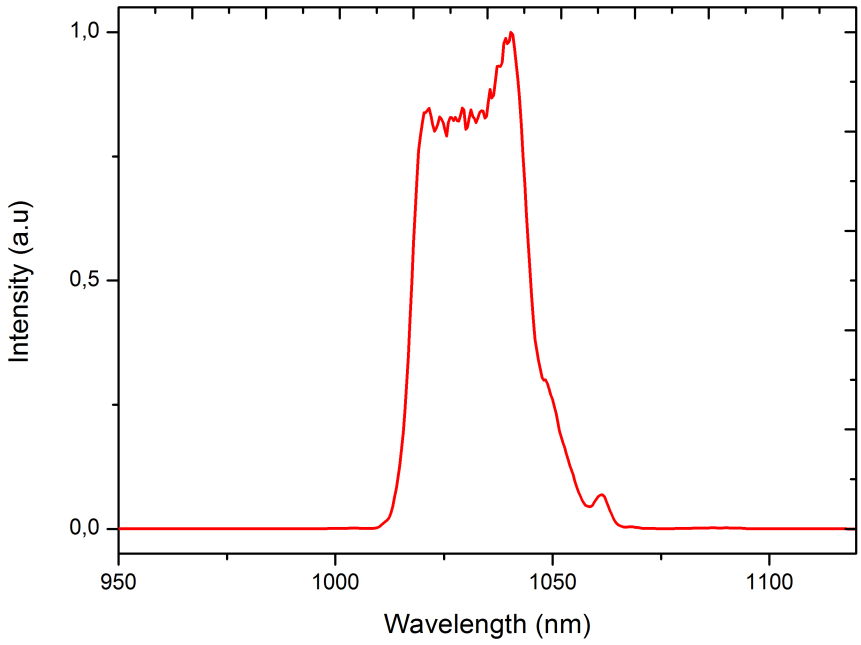

Figure 4.8: Measured spectra obtained from the power amplifier output

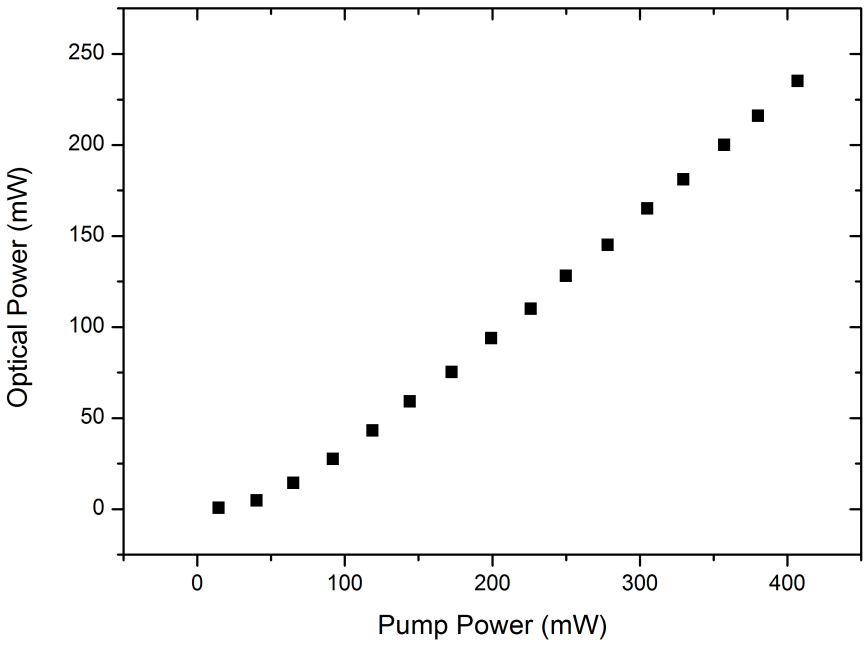

Figure 4.9: Measured signal power as a function of pump power

measurement is important for Yb-doped fiber laser as source of a THz-TDS system. The power fluctuation is below 1.0 % which is quite stable for THz measurements.

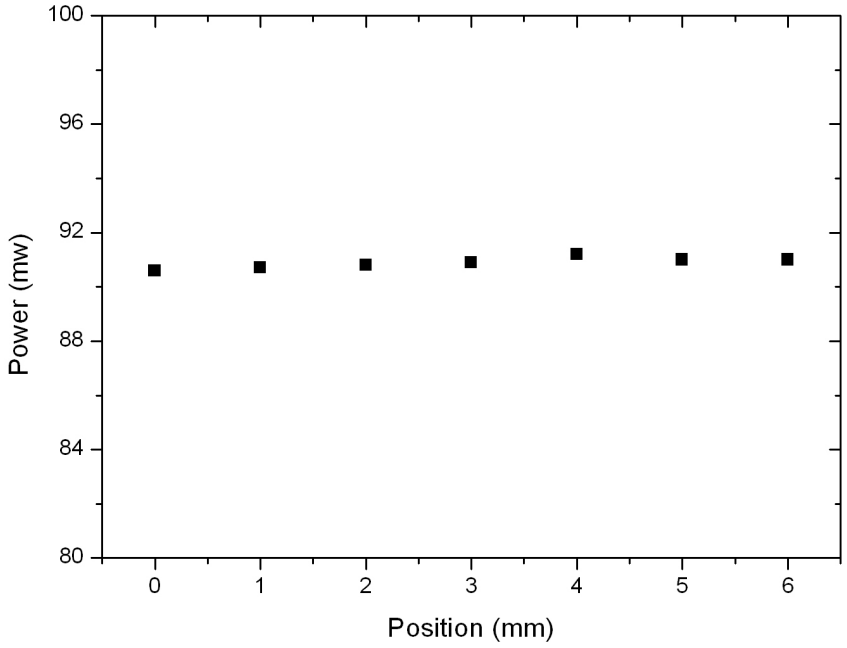

Figure 4.10: Power stability of the amplifier output

Power and pulse duration stability over time are also studied. For five hours with one hour intervals, average power output and pulse duration were observed to be stable.

4.3 THz-TDS MEASUREMENTS AT DIFFERENT REPETITION-RATES OF FIBER LASER

Firstly, the system displayed in Figure 3.2 was tested with Ti:Al_2O_3 laser at 780 nm central wavelength in order to achieve equal length of generation and detection arm. After this condition was met, this system is modified for 1031 nm central wavelength of Yb-doped fiber laser. First one is to maintain a linearly polarized light before beam splitter (BS). Although PM components are used in pre-amplifier part, to eliminate orthogonal polarization components, combination of half wave plate and polarizing beam splitter (PBS) was used. Transmitted light from PBS was horizontally polarized.

Therefore, photoconductive antenna is placed according to this orientation. Mirrors used were broadband dielectric mirrors that work for 1031 nm. Mirror 6, 7 and corner cube were metallic mirrors. Luckily, input power was distributed according to plan. 35 mW after PBS were distributed 26 mW to 6.6 mW by BS for generation and detection arms respectively. Hence, no filter was needed to attenuate arms not to damage PCA and balanced photo detector. Detection arm focusing lens were changed from A coating to C coating lens for 1031 nm. GaP and ZnTe Both crystals can be used in electro optic detection. Signal power is proportional to crystal thickness while broader bandwidth can be achieved with GaP for about 1 μm wavelength [60]. One of our main challenge was that the collimation of pre-amplifier. This parameter was related with the beam diameter arriving to PCA. According to data sheet of PCA, acceptance beam diameter should be 5 mm at most. In our case, this was larger than 5 mm; therefore, all power arriving PCA cannot be coupled to dipole structure. In order to compensate this effect, C coating lens with 175 cm of focal length is used to couple all light to PCA. Position of this lens is optimized so that it is placed to an arbitrary point. Our main limitation was that a silicon based balanced photo detector is used in detection arm. For larger wavelength than 1 μm, the response of detector decreases greatly. This can be improved by two ways. An InGaAs based balanced detector can be used for higher response. Second way is that antenna-antenna system can be constructed to overcome detector handicap. In this method, bandwidth would be limited to antenna characteristics.

In modified PCA-ZnTe crystal THz-TDS system, three measurements are carried for 3 different repetition rates in order to observe the stability of THz generation. THz signals of these measurements are displayed in Figure 4.11-4.13.

Fourier transformations of these signals are displayed in Figure Figure 4.14 in order to compare spectrum stability of measurements.

According to measurements, a high signal to noise ratio could not be achieved. The slight change in THz signal and power spectrum can be observed. However, first position corresponds to between second and last measurement. Thus, it can be deduced that the change in THz signals and power spectrum is caused by low signal to noise ratio not repetition rate tuning. In THz waveform measurement, a pre-signal is observed

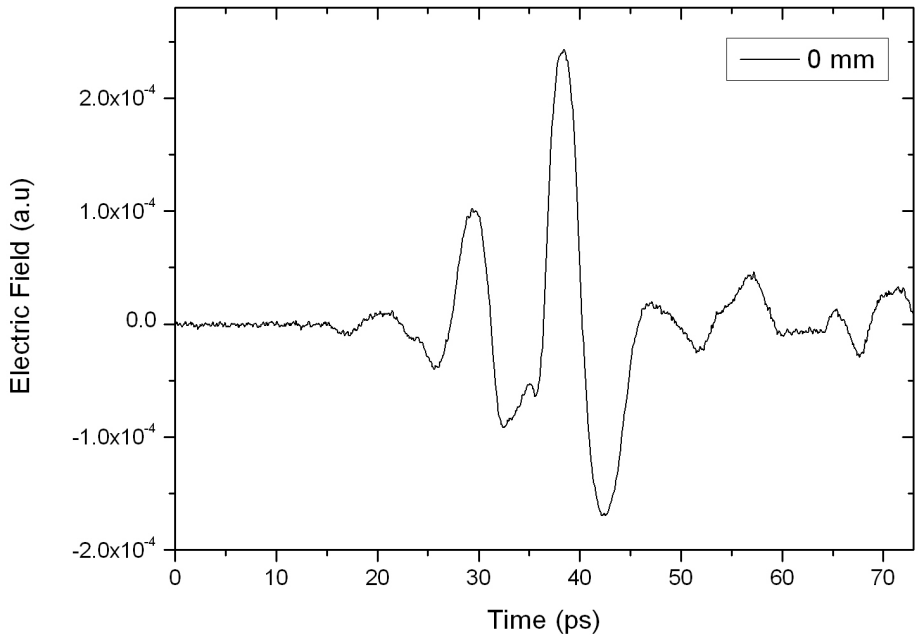

Figure 4.11: THz signal for 0 mm oscillator scan stage position

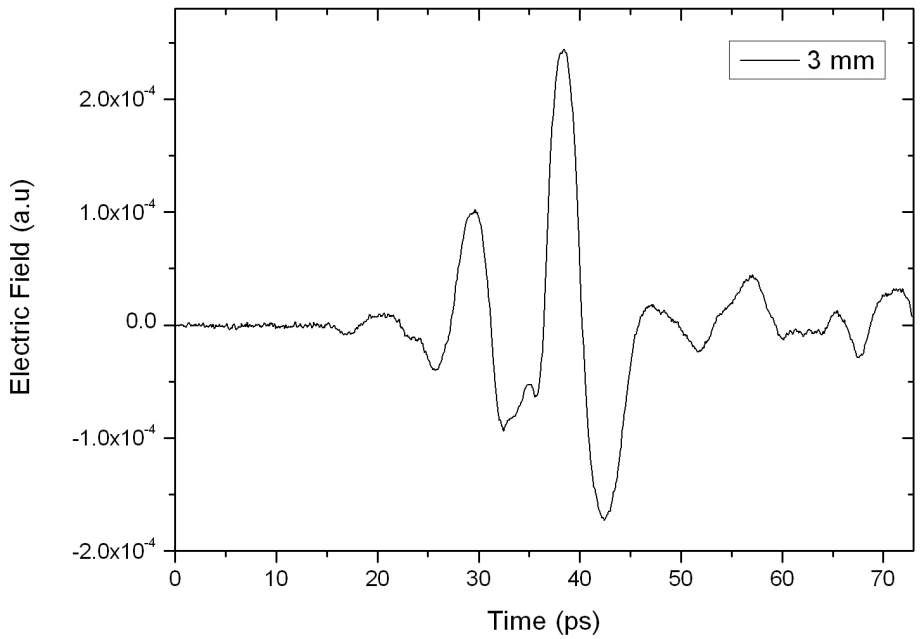

Figure 4.12: THz signal for 3 mm oscillator scan stage position

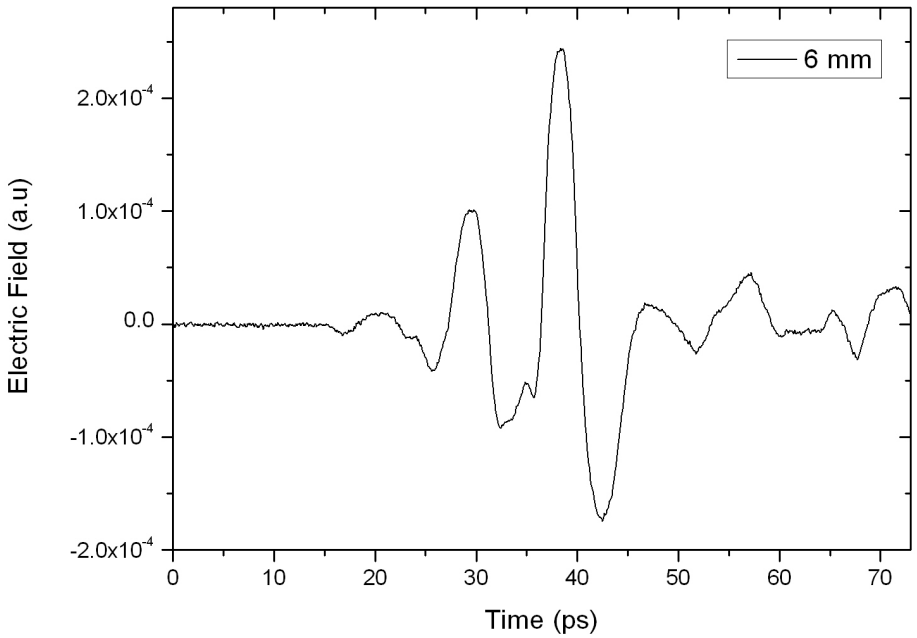

Figure 4.13: THz signal for 6 mm oscillator scan stage position

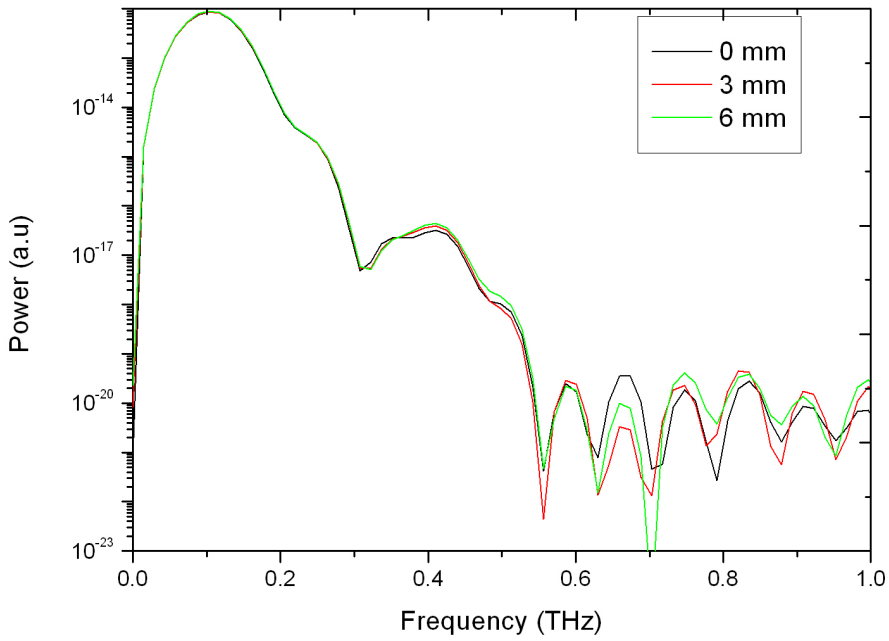

Figure 4.14: Power spectra of the THz signals for different scan stage position

before the main peak. This is mainly caused by the inner reflection in the thin beam splitter which causes a decrease in power spectrum. This pre-pulse can be eliminated by using a thicker beam splitter.

CHAPTER 5

CONCLUSION

In this study, the development of a THz-TDS system driven by a novel Yb-doped fiber laser pre-amplified laser whose repetition rate can be tuned is discussed specifically for fast scan THz measurements. Traditionally THz-TDS systems use linear stages alter time delay between generation and detection arms. This interferometric process takes more ten minutes due to integration times. Several techniques are developed to accelerate this process. The main goal of this study is that home-build Yb-doped fiber oscillator can be used in OSCAT technique as an alternative method for fast scan THz measurements. To support this idea, stability of oscillator is examined in terms of power, spectrum and pulse duration at different repetition rates of laser. Afterwards, THz waveforms at different rep-rates are measured for additional verification.

A general introduction about the fiber lasers and terahertz time domain spectroscopy is given in chapter one. Then, in order to understand the basics of fiber laser, theoretical background of fiber lasers are summarized including optical fibers, basic of nonlinear optics, dispersion, pulse propagation in fiber, mode locking theory in chapter two. Additionally, repetition-rate tuning of oscillator which is related to OSCAT technique is explained. Final part of chapter two gives system overview of Yb-doped fiber laser. Third chapter covers the THz-TDS with antenna generation. First part of this chapter explains the generation and detection technique used in this thesis. Then THz-TDS system overview is given in next part including data collection data collection procedure. At the end, data analysis and theoretical approach is given.

Forth chapter covers the measurements for this thesis. The Yb-doped laser system consisted of two main parts which were oscillator and amplifier. Passively mode-locked

Yb-doped fiber laser oscillator used NPE used as a saturable absorber technique to achieve mode-lock condition. This oscillator delivers pulses at average power of 15 mW at central wavelength of 1042 nm with 35 nm bandwidth at 51 MHz. Repetition rate tuning of oscillator is examined to observe the stability of laser. According to calculated OSCAT parameters, scanning 6 mm of oscillator tuned repetition rate of about 53 kHz over about 51.6 MHz. Repetition rate is changed linearly at each 1 mm tuning step. This tuning range can cover over 100 ps time window in OSCAT/THz-TDS measurements.

Afterwards, pre-amplifier part is studied in terms of pulse duration, spectrum and power stability. Pre-amplifier delivers over 90 mW at the central wavelength of 1031 nm. Power fluctuation with rep-rate tuning is lower than 1 % with 4 % change in pulse duration over about 82 fs. These results are lower than the OSCAT with Er-doped fiber laser [39]. According to these parameters, great dynamic range can be achieved with an optimized THz-TDS system.

In the final section of chapter four, preliminary THz-TDS measurements are given. Our spectroscopy system has bandwidth about 0.1 to 0.5 THz. S/N is about 60. THz waveform measurement is repeated for different repetition rates of Yb-doped fiber oscillator in order to study this system for OSCAT technique in terms of stability. Cavity length of oscillator is altered 6 mm to tune repetition rated about 50 kHz over 51 MHz. Although THz waveform and power spectrum changes at each oscillator scan position, an optimized system can achieve better results. In order to upgrade system, a InGaAs balanced detector can be implemented instead of silicon based detector. Another solution to response problem for 1 μm wavelength is to modify system to antenna generation-antenna detection system. Therefore, there will not be a need for balanced detector. In future works, these solutions will be carried to achieve better results.

In conclusion, stability of Yb-doped fiber laser shows that the system can be used in OSCAT technique as source to scan the THz waveform without the use of any external delay lines. However, THz-TDS measurements should be improved by necessary improvements in spectrometer as mentioned earlier. In OSCAT, the data acquisition is based on a novel method where the laser cavity repetition rate is tuned over the entire

THz waveform thereby shortening the data acquisition times throughout the measurements. The oscillator for the amplified Yb-doped fiber laser system was constructed with a repetition rate of 51 MHz. For OSCAT technique, additional pre-amplifier system with a passive delay line should be constructed. To scan a length of 100 ps the cavity needs to be tuned over $\pm$ 25 kHz, for which the laser system exhibited little or no difference in output pulse duration, power and spectrum characteristics which is a testament to the stability of these lasers compared to other solid-state mode-locked lasers. Using this technique, scan times of obtaining one THz waveform for THz-TDS measurements is less than one minute.

Additionally, the importance of this system is realized in that Yb-doped fiber lasers can be amplified to sub-millijoule pulse strengths more easily than other types of fiber lasers. Coupled with measurement techniques developed in OSCAT technique, an amplified Yb-doped fiber laser driven THz-TDS system can perform pump/probe measurements in a more compact and robust platform. This will allow for rapid measurements of THz pulse profiled which will be essential for scanning the entire THz waveform through the excited sample, a technique commonly referred to as 2D-scan excite/THz probe measurements.

REFERENCES

[1] Y. S. Lee, "Principles of Terahertz Science and Technology," Springer Science+Business Media, LLC, (2009).

[2] I. Jones, T. J. Rainsford, B. Fisher, and D. Abbott, "Towards T-ray spectroscopy of retinal isomers: A review of methods and modeling," Vibrational Spectroscopy 41, 144-154 (2006).

[3] K. Sakai, and M. Tani, "Introduction to Terahertz Pulses," K. Sakai (Ed.): Terahertz Optoelectronics, Topics Appl. Phys., 97, 1-30 (2005).

[4] D. F. Plusquellic, K. Siegrist, E. L. Heilweil, and O. Esenturk, "Applications of Terahertz Spectroscopy in Biosystems," Chem. Phys. Chem. 8, 2412-2431 (2007).

[5] X. C. Zhang, and J. Xu, "Introduction to THz Wave Photonics," Springer Science+Business Media, LLC, (2010).

[6] J. L., British Patent 285, 738 (1928).

[7] C. W. Hansell, U.S Patent 1, 751,584 (1930).

[8] H. Lamm, "Biegsame optische gerate," Z. Instrumenten. 50, 579 (1930).

[9] A. C. S. van Heel, "A new method of transporting optical images without aberrations," Nature 173, 39 (1954).

[10] H. H. Hopkins, and N. S. Kapany, "A flexible fiberscope using static scanning," Nature 173, 39 (1954).

[11] B. O'Brian, U. S. Patent 2,825,260 (1958).

[12] B. I. Hirschowitz, U. S. Patent 3,010,357 (1961).

[13] T. Miya, Y. Terunuma, T. Hosaka, and T. Miyashita, "Ultimate low-loss single-mode fibre at 1.55 μm," Electron. Lett. 15, 106 (1979).

[14] Fiber Optics for Sale, http://www.fiberoptics4sale.com/wordpress/optical-fiber-attenuation, last visited 12/07/2013.

[15] R. H. Stolen, E. P. Ippen, and A. R. Tynes, "Raman oscillation in glass optical waveguide," Appl. Phys. Lett. 20, 62 (1972).

[16] E. P. Ippen, and R. H. Stolen, "Stimulated Brillouin scattering in optical fibers," Appl. Phys. Lett. 21, 539 (1972).

[17] R. G. Smith, "Optical power handling capacity of low loss optical fibers as determined by stimulated Raman and Brillouin scattering," Appl. Opt. 11, 2489 (1972).

[18] R. H. Stolen and A. Ashkin, "Optical Kerr effect in glass waveguide," Appl. Phys. Lett. 22, 294 (1973).

[19] R. H. Stolen, J. E. Bjorkholm, and A. Ashkin, "Phase-matched three-wave mixing in silica fiber optical waveguides," Appl. Phys. Lett. 24, 308 (1974).

[20] K. O. Hill, D. C. Johnson, B. S. Kawasaki, and R. I. MacDonald, "CW three-wave mixing in single-mode fibers," J. Appl. Phys. 49, 5098 (1974).

[21] R. H. Stolen, "Phase-matched-stimulated four-photon mixing in silica-fiber waveguides," IEEE J. Quantum Electron. QE-11, 100 (1975).

[22] R. H. Stolen, and C. Lin, "Self-phase-modulation in silica optical fibers," Phys. Rev. A 17, 1448 (1978).

[23] A. Hasegawa, and F. Tappert, "Transmission of stationary nonlinear optical pulses in dispersive dielectric fibers. I. Anomalous dispersion," Appl. Phys. Lett. 23, 142 (1973).

[24] L. F. Mollenauer, R. H. Stolen, and J. P. Gordon, "Experimental observation of picosecond pulse narrowing and solitons in optical fibers," Phys. Rev. Lett. 45, 1095 (1980).

[25] I. N. Duling III, "Subpicosecond all-fibre erbium laser," Electron. Lett. 27, 544-545 (1991).

[26] K. Tamura, C. R. Doerr, H. A. Haus, and E. P. Ippen, "Soliton fiber ring laser stabilization and tuning with a broad intracavity filter," IEEE Phot. Tech. Lett. 6, 697-699 (1994).

[27] K. Tamura, E. P. Ippen, H. A. Haus, and L. E. Nelson, "77-fs pulse generation from a stretched-pulse mode-locked all-fiber ring laser," Opt. Lett. 18, 1080-1082 (1993).

[28] F. Ö. Ilday, J. R. Buckley, W. G. Clark, and F. W. Wise, "Self-similar evolution of parabolic pulses in a laser," Phys. Rev. Lett. 92, 3902-3905 (2004).

[29] J. R. Buckley, F. Ö. Ilday, and F. W. Wise, "Femtosecond fiber lasers with pulse energies above 10 nJ," Opt. Lett. 30, 1888-1890 (2005).

[30] A. Chong, J. Buckley, W. Renninger, and F. Wise, "All-normal-dispersion femtosecond fiber laser," Opt. Exp. 14, 10095-10100 (2006).

[31] B. Oktem, C. Ülgüdür, and F. Ö. Ilday, "Soliton-similariton fibre laser", Nat. Photonics, 4, 307, (2010).

[32] E. Snitzer, H. Po, F. Hakimi, R. Tumminelli, B. C. McCollum, "Double clad offset core Nd fiber laser", Optical Fiber Sensors Topical Meeting, New Orleans, Louisiana/USA, paper PD 5, (1988).

[33] IPG Photonics, http://www.ipgphotonics.com, last visited 12/07/2013.

[34] G. Mourou, C. V. Stancampiano, A. Antonetti, and A. Orszag "Picosecond microwave pulses generated with a subpicosecond laser-driven semiconductor switch," Appl. Phys. Lett., 39, 4, 295-296 (1981).

[35] S. L. Dexheimer, "Terahertz Spectroscopy: Principles and Applications" CRC Press, (2008).

[36] G.-J. Kim, S.-G. Jeon, J.-I. Kim,Y.-S. Jin, "Terahertz pulse detection using rotary optical delay line," Jpn. J. Appl. Phys. 46 (2007).

[37] G. Chang, C. J. Divin, C.-H. Liu, S. L. Williamson, A. Galvanauskas, and T. B. Norris, "Power scalable compact THz system based on an ultrafast Yb-doped fiber amplifier," Opt. Exp., 14, 17, 7909-7913 (2006).

[38] T. Yasui, E. Saneyoshi, T. Araki, "Asynchronous optical sampling terahertz time-domain spectroscopy for ultrahigh spectral resolution and rapid data acquisition," Appl. Phys. Lett. 87, 6 (2005).

[39] T. Hochrein, R. Wilk, M. Mei, R. Holzwarth, N. Krumbholz, and M. Koch, "Optical sampling by laser cavity tuning," Opt. Exp. 18, 1613-1617 (2010).

[40] P. V. Mamyshev, S. V. Chernikov, and E. M. Dianov, "Generation of fundamental soliton trains for high-bit-rate optical fiber communication lines" IEEE J Quantum Electron 27:2347–2355 (1991).

[41] M. Miyamoto, M. Tsuchiya, H.-F. Liu, and T. Kamiya, "Generation of ultrashort (65 fs) pulses from 1.55 μm gain-switched distributed feedback (DFB) laser with soliton compression by dispersion arrangement" Jpn. J. Appl. Phys. 35:L1330–L1332 (1996).

[42] M. Hofer, M. E. Fermann, A. Galvanauskas, D. Harter, and R. S. Windeler, "High-power 100 fs pulse generation by frequency doubling of an erbium-ytterbium fiber master oscillator power amplifier," Opt. Lett. 23:1840–1842 (1998).

[43] A. Galvanauskas, M.E. Fermann, P. Blixt, Jr J. A. Tellefson, and D. Harter, "Hybrid diode-laser fiber-amplifier source of high-energy ultrashort pulses," Opt. Lett. 19:1043–1045 (1994).

[44] A. Galvanauskas, Z. Sartania, and M. Bischoff, "Millijoule femtosecond all-fiber system. Conf. on Lasers and Electro-Optics," CLEO, 2001, Paper CMA-1.

[45] G. P. Agrawal, Nonlinear Fiber Optics. San Diego, CA, USA: Elsevier Inc., (2007).

[46] D. Milam, "Review and assessment of measured values of the nonlinear refractive-index coefficient of fused silica," Appl. Opt., 37, 3, 54-550 (1998).

[47] M. R. Hee, J.A. Izatt, J.M. Jacobson, J.G. Fujimoto, and E.A. Swanson, "Femtosecond transillumination optical coherence tomography," Opt. Lett. 18, 950-952 (1993).

[48] M. J. Stevens, A. L. Smirl, R. D. R. Bhat, J. E. Sipe, and H. M. van Driel, "Coherent control of an optically injected ballistic spin-polarized current in bulk GaAs," J. Appl. Phys., 91, 7, 4382 - 4386 (2002).

[49] C. A. Schmuttenmaer, "Exploring dynamics in the far-infrared with terahertz spectroscopy," Chem. Rev., 104, 1759-1779 (2004).

[50] F. Liu, Y.-J. Song, Q.-R. Xing, M.-L. Hu, Y.-F. Li, C.-L. Wang, L. Chai, W.-L. Zhang, A. M. Zheltikov, and C.-Y. Wang, "Broadband Terahertz Pulses Generated by a Compact Femtosecond Photonic Crystal Fiber Amplifier," IEEE Photon. Technol. Lett., 22, 11, 814-816 (2010).

[51] Q. Wu, and X.-C. Zhang, "Free-space electro-optic sampling of terahertz beams" Appl. Phys. Lett. 67, 24, 3523- 3525 (1995).

[52] G. Gallot, and D. Grischkowsky, "Electro-optic detection of terahertz radiation," J. Opt. Soc. Am. 16, 8, 1204-1212 (1999).

[53] A. Nahata, and H. Cao, "Broadband phase-matched generation and detection of terahertz radiation" Proceedings of SPIE 5411, 150-157 (2004).

[54] A. Nahata, D. H. Auston, T. F. Heinz, and C. Wu, "Coherent detection of freely propagating terahertz radiation by electro-optic sampling" Appl. Phys. Lett. 68, 8, 150-152 (1996).

[55] Batop, http://www.batop.com/products/terahertz/photoconductive-antenna/data-sheet/manual_PCA-40-05-10-1060.pdf, last visited 12/07/2013.

[56] CVI Melles Griot, http://search.newport.com/?q=*&x2=sku&q2=PARAB-3, last visited 12/07/backslash/2013.

[57] Stanford Research Systems, http://www.thinksrs.com/downloads/PDFs/Manuals/SR830m.pdf, last visited 12/07/2013.

[58] P.U. Jepsen, and B.M. Fischer, "Dynamic range in terahertz time-domain transmission and reflection spectroscopy," Opt. Lett. 30, 1, 29-31 (2005).

[59] K. Ozgoren, B. Oktem, S.Yılmaz, K. Eken, and F. O. Ilday, "83W, 3.1 MHz, square-shaped, 1 ns-pulsed all-fiber-integrated laser for micromachining" Opt. Exp. 19, 17647 (2011).

[60] B. Pradarutti, G. Matthaus, C. Brückner, J. Limpert, S. Riehemann, G. Notni, S. Nolte, and A. Tunnermann, "Electrooptical sampling of ultra-short THz pulses by fs-laser pulses at 1060 nm," Appl. Phys. B 85, 59–62 (2006).